Miner Deposita (2012) 47:129–150
DOI 10.1007/s00126-011-0348-5

ARTICLE

Platinum group element and nickel sulphide ore tenors of the Mount Keith nickel deposit, Yilgarn Craton, Australia

Stephen J. Barnes · Marco L. Fiorentini · Michael C. Fardon

Received: 7 July 2010 / Accepted: 15 March 2011 / Published online: 15 May 2011

Abstract A set of platinum group element (PGE) analyses of about 120 samples from a 250-m continuous drill core through the Mount Keith komatiite-hosted nickel orebody, combined with Ni, Cu, Co, S, and major elements, reveals a complex trend of covariance between the original cumulus components of a thick sequence of nearly pure olivine–sulphide liquid adcumulates. The intersection is divided into informal chemostratigraphic zones, defined primarily by combinations of fine-scale cyclicity in original olivine composition, defined by Mg#, and sulphide composition, defined by Pt/S and Ni/S. Contents of Ni and PGE in 100% sulphides (tenors) were determined from linear regressions of the Ni–S and PGE–S covariance for each zone. Inferred olivine compositions range from about Fo_{92} to $Fo_{94.6}$ and show a broad decrease from bottom to top of the sequence complicated by numerous reversals, revealing crystallisation in an open conduit system. Ni and PGE tenors of Mount Keith sulphide ores have typical values similar to the type I deposits of the Kambalda Dome. Mobility of S, at least on the scale of 2-m sample composites, is evidently relatively minor. Tenors for the various zones range 12–22% Ni, 370–1540 ppb Pt, 970–3670 ppb Pd, 100–460 ppb Ir, 170–460 ppb Rh, and 710–1260 ppb Ru. Pt, Pd, and Rh tenors are very strongly correlated, but the iridium group of platinum group elements (IPGEs; Ir and Ru) less so. Tenor variations are predominantly controlled by variations in magma/sulphide ratio R (100–350), with a minor component of variance from equilibrium crystallisation trends in the parent magma. PGE depletion in the silicate melt due to sulphide liquid extraction is limited by entrainment of sulphide liquid droplets and continuous equilibration with the transporting silicate magma. Ratios of the PGEs to one another are similar to those in the host komatiite magma, with the exception of Pt, which is systematically depleted in ores, relative to Rh and Pd and relative to host magma, by a consistent factor of about 2 to 2.5. This anomalous Pt depletion relative to PGE element ratios in unmineralized komatiitic rocks matches that observed in bulk compositions of many komatiite-hosted orebodies. The highly consistent nature of this depletion, and particularly the very strong correlation between Pt, Pd, and Rh in the Mount Keith deposit, argue that this depletion is a primary magmatic signal and not an artefact of alteration. Differential diffusion rates between Pt and the other PGEs, giving rise to a low effective partition coefficient for Pt into sulphide liquid, is advanced as a possible but not definitive explanation.

Keywords Komatiites · Magmatic sulphides · Platinum group elements · R factor · Adcumulates · Dunites · Nickel · Mount Keith · Western Australia · Yilgarn

Editorial handling: C. Michael Lesher

S. J. Barnes (✉)
CSIRO Earth Science and Resource Engineering,
Kensington,
Perth 6151 WA, Australia
e-mail: steve.barnes@csiro.au

M. L. Fiorentini
Centre for Exploration Targeting, University of Western Australia,
Crawley, WA 6009, Australia

M. C. Fardon
Department of Earth Sciences, Monash University,
Clayton, VIC, Australia

Present Address:
M. C. Fardon
URS Australia Pty Ltd.,
Level 4, 70 Light Square,
Adelaide, South Australia 5000, Australia

Introduction

The platinum group elements (PGE) are important economic constituents of magmatic sulphide ores, and their parts per billion- to parts per million-level concentrations in magmatic sulphides are useful as indicators of ore-forming processes. A large body of data have been accumulated over the last three decades on PGE contents of magmatic sulphide ores associated with komatiites (e.g. Keays and Davidson 1976; Ross and Keays 1979; Keays et al. 1981, 1982; Lesher and Keays 1984; Cowden et al. 1986; Barnes and Naldrett 1987; Barnes et al. 1988; Barnes and Giovenazzo 1990; Lesher and Campbell 1993; Heath et al. 2001; Barnes 2004), but with the exception of datasets on Mount Keith (Ross and Keays 1979; Keays 1982), Dumont (Brugmann et al. 1990), Perseverance (Barnes et al. 1988), and Black Swan (Barnes 2004; Barnes et al. 2009); most of the available data have been collected from sulphide-rich deposits at the base of komatiitic flows or intrusions, the so-called type I deposits (Lesher 1989; Hill and Gole 1990; Lesher and Keays 2002). This study describes the PGE distribution within the Mount Keith deposit, the type example of the so-called type II deposits, defined as centrally disposed accumulations of weakly disseminated Fe–Ni sulphides within komatiitic dunite bodies (Lesher and Keays 2002; Barnes 2006; Grguric et al. 2006).

Disseminated ores are of particular interest in that they potentially preserve primary magmatic compositions of magmatic sulphide liquids, unmodified by the process of monosulphide solid solution (MSS) fractionation or other magmatic differentiation mechanisms that induce compositional variance within the ore. This advantage comes at a price, however, in that determination of the composition of the sulphide liquid component of the rock (metal tenors = original concentration of metals in 100% sulphides) is complicated by the presence of ore-forming elements in the non-sulphide fraction of the rock. In the case of Ni, and possibly Ir and Ru, the non-sulphide component of the rock contains a significant proportion of the whole rock element budget, and this propagates large uncertainties into sulphide tenor estimates. This limitation has restricted the amount of reliable data on compositions of the sulphide component of type II ores, as has the potentially large effect of element redistribution during hydrothermal alteration (Eckstrand 1975; Groves and Keays 1979; Donaldson 1981; Grguric et al. 2006; Barnes et al. 2009). In this contribution, this problem is addressed using previously published high-precision Ni sulphide fire assay, ICP-MS data on a diamond drill core intersecting the entire Mount Keith orebody, by investigating detailed whole rock inter-element correlations within empirically selected stratigraphic zones of the orebody. These results lead into a broader discussion of the relationship between PGE concentrations in associated silicate and sulphide magmas.

Geological setting

Mount Keith is situated in the northern part of the Agnew-Wiluna Domain (also commonly called the Agnew-Wiluna Greenstone Belt) which forms the northern section of the Kalgoorlie Terrane of the Eastern Goldfields Province of the Yilgarn Craton of Western Australia (Hill et al. 1995, 2001; Beresford et al. 2004). The Agnew-Wiluna Domain comprises a ca. 2.7 Ga sequence of felsic-to-intermediate volcanic and volcaniclastic rocks, sulfidic cherts, carbonaceous shales, and laterally variable komatiites including cumulates, thin spinifex-textured units, and komatiitic basalts. The Agnew-Wiluna Domain is one of the most highly Ni-endowed belts in the world (Hronsky and Schodde 2006; Barnes et al. 2007) and contains several world-class Ni–Cu–(PGE) deposits, including two of the largest known komatiite-hosted ore deposits at Mount Keith and Perseverance (Fig. 1). The Mount Keith deposit is the world's largest accumulation of magmatic sulphide-hosted nickel within rocks of komatiitic affinity, with a pre-mining resource of 503 million tonnes of ore at a grade of 0.55% Ni for 2,770,000 tonnes of contained Ni (Barnes 2006).

The Mount Keith domain (Fig. 1) contains three ultramafic horizons from stratigraphic bottom to top: (1) the Mount Keith Ultramafic unit (MKU), (2) the Cliffs Ultramafic unit (CLU), and (3) the Monument Ultramafic

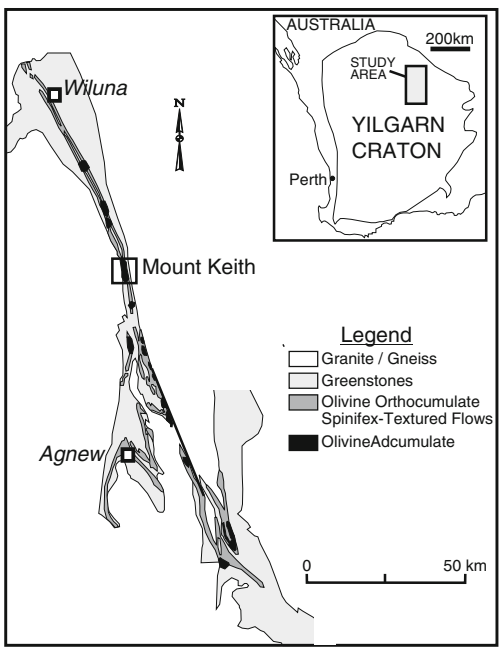

Fig. 1 Location map and regional geology of Mount Keith area, after Fiorentini et al. (2007)

unit (MU). The three ultramafic belts are separated by a variably deformed sequence of felsic and mafic rocks, ranging in composition from dacite to Mg-rich tholeiitic basalts. The MKU contains the type II mineralization which is the topic of this study. The CLU contains the Cliffs deposit, a type I basal massive sulphide accumulation within channelized compound komatiite flows, whereas the MU comprises thin differentiated spinifex-textured komatiite flows with no known sulphide mineralization. Platinum group element concentrations in sulphide-free MU flows were reported by Dowling and Hill (1992).

The volcanological architecture of the Mount Keith Ultramafic Complex is interpreted as a subhorizontal, subvolcanic sill comprising a central conduit acting as a feeder to overlying komatiite flows (Rosengren et al. 2005, 2007; Fiorentini et al. 2007). The internal architecture of the MKU is made up of adcumulate-textured pods and lenses, which are flanked by laterally extensive meso- and orthocumulate-textured units (Dowling and Hill 1993; Fiorentini et al. 2007; Rosengren et al. 2007). Disseminated Fe–Ni–(Cu) sulphide blebs occur interstitial to former olivine crystals and are concentrated in the lensoidal bodies. The internal stratigraphy in the thickest part of the body, as represented by the drill core described here, consists almost entirely of extreme olivine adcumulates, with Al_2O_3 contents commonly <0.25%, with a thin orthocumulate base and intervals of transitional adcumulate to mesocumulate in the upper half of the body, truncated by a major shear zone separating the complex from hanging wall dacites (Fig. 2).

Analytical methods

The data investigated in this study were originally collected as part of an Honours student thesis (Fardon 1995) and have previously been reported by Fiorentini et al. (2007). Samples were collected from diamond drill hole MKD153, which intersected the entire thickness of the thickest part of the orebody in the core of the dunite lens (Fig. 2). Samples were collected as 2-m aggregates of halved drill core during the original ore delineation programme carried out by WMC Resources and were analysed at Analabs Laboratories, Perth, WA, in 1995. Average analyses by stratigraphic zone are given in Table 1.

PGEs were analysed by Ni sulphide fire assay with ICP-MS finish. Details of analytical precision based on replicate analyses of WMC Resources reference materials analysed by Analabs over the period of the original thesis work, taken from

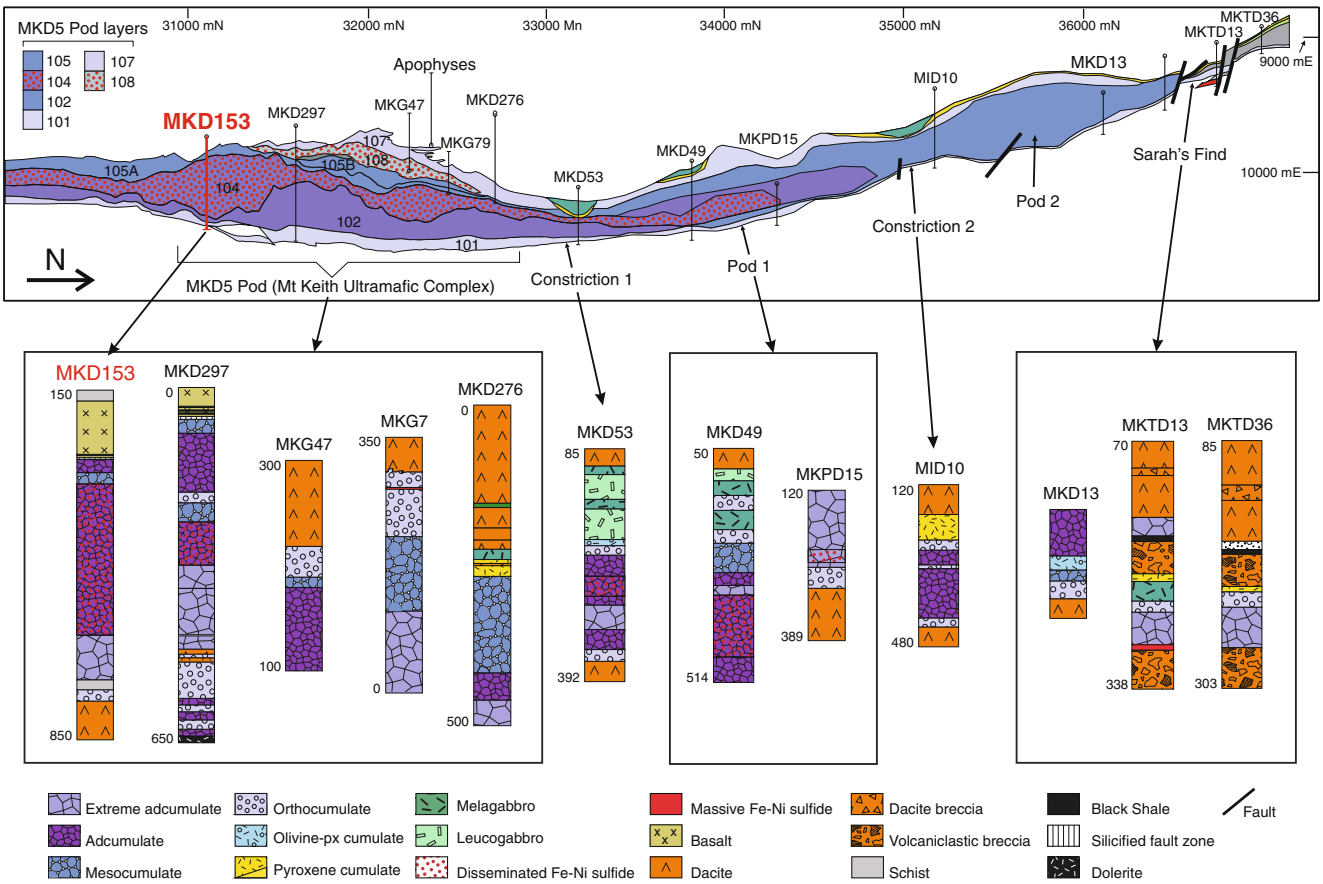

Fig. 2 Detailed geology of the Mount Keith ultramafic complex showing location of study hole MKD153, after Fiorentini et al. (2007)

Table 1 Average whole rock analytical data by stratigraphic subzone

	Zone A	Zone B	Zone C	Zone D	Zone E	Zone F
SiO_2	41.8	41.5	42.2	42.3	42.0	40.0
TiO_2	0.0	0.0	0.0	0.1	0.0	0.0
Al_2O_3	0.5	0.3	0.3	1.4	0.3	0.2
FeO	7.0	6.6	6.0	6.5	6.6	6.4
Fe_2O_3	0.1	0.1	0.1	0.1	0.1	
MnO	0.1	0.1	0.1	0.1	0.1	0.1
MgO	49.4	50.3	49.9	47.8	50.1	52.2
CaO	0.7	0.7	0.5	1.0	0.2	0.4
Na_2O	0.1	0.1	0.1	0.1	0.1	0.1
K_2O	0.0	0.0	0.0	0.2	0.0	0.0
S	1.2	1.5	1.3	1.3	1.2	0.4
Mg#	92.5	93.0	93.5	92.7	93.0	93.5
M/Si	1.9	1.9	1.9	1.8	1.9	2.1
Ni	5,536	7,704	9,547	7,330	7,638	5,235
Cu	239	292	334	225	212	36
Co	173	215	214	179	194	146
Cr	1,229	1,124	1,069	1,059	1,236	982
Ir	13.0	15.4	16.9	15.2	16.0	16.2
Ru	22.0	33.9	28.9	26.9	26.5	18.8
Rh	5.1	8.3	8.3	7.7	7.6	6.3
Pt	11.1	22.4	25.3	23.8	22.1	17.3
Pd	28.6	56.4	57.8	53.7	52.1	40.1
Samples	23	26	24	19	14	15

Data recalculated to 100% volatile-free (see "Analytical methods"). Fe_2O_3 calculated using the MgO-dependent formulation of Barnes et al. (2007)

Brand (1997), are given in Table 2. Other elements were analysed by XRF, except S which was analysed by Leco induction furnace with a detection limit of 5 ppm.

A set of six samples was collected by resampling the original drill core in the form of 50-cm intervals of contiguous quarter core from within matching intervals. These samples are not strictly replicates in that they are subsamples from within originally larger intervals and represent physically distinct samples from the opposite half of the drill core, and hence cannot be used conclusively to establish precision or accuracy given the decimetre-scale heterogeneity of sulphide distribution within the samples. However, they gave a good indication of reproducibility, particularly for element ratios which would be expected to be independent of sulphide abundance. These samples were analysed by ICP-MS following Ni sulphide fire assay preconcentration and tellurium co-precipitation by Dany Savard in Prof. Sarah-Jane Barnes' laboratory at the University of Quebec at Chicoutimi. Results are given in Table 3, which documents the comparison with the corresponding original sample interval. Median values for relative difference between the Analabs and UQAC datasets are around 25–30% for all elements and PGE ratios, except for Pt/Pd which agree in all cases to better than 20%, with a median relative difference of 12%. These results confirm the quality of the Analabs data.

Table 2 Summary of replicate analyses on internal reference material AB803701 (partially oxidised ultramafic rock from Mount Keith supplied by WMC Resources)

Element	Ir	Os	Ru	Rh	Pt	Pd
Detection limit (ppb)	1	1	1	1	1	1
Expected result (ppb)	35	43	123	36	15	68
Precision (±%)	8	9	9	9	13	7
Accuracy (%)	10	−2	−6	16	−2	−1
Mean (ppb)	39	42	116	42	15	67
Standard deviation	2	2	5	2	1	2
Minimum (ppb)	36	39	108	39	13	64
Maximum (ppb)	41	46	124	45	16	72
n	11	11	11	11	11	11

Replicate analyses at Analabs Laboratory, Perth, WA, 1995–1997, by Ni sulphide fire assay with ICP-MS finish. Data from Brand (1997)

The MKD153 profile

Petrography of samples

Detailed accounts of the hypogene mineralogy of the Mount Keith orebody are given by Rödsjö (1999) and

Table 3 Comparison of analytical data for PGEs from Analabs (2-m sample intervals) and 40-cm grab samples from within the same intervals analysed at the University of Quebec at Chicoutimi by Ni sulphide fire assay with ICP-MS finish

Sample	Lab/year	Ru	Rh	Pd	Os	Ir	Pt	Pt/Pd	Pt/Rh	Pd/Ir
Analyses of corresponding samples (ppb)										
MKD153-514.6	UQAC 2010	17.3	5.6	46.9	12.6	9.6	18.6	0.4	3.3	4.9
MKD153-513-515	Analabs 1995	23.0	7.0	37.0		11.0	16.0	0.4	2.3	3.4
MKD153-644.5	UQAC 2010	24.1	7.1	56.2	16.5	12.5	27.8	0.5	3.9	4.5
MKD153-643-645	Analabs 1995	21.0	8.0	54.0		19.0	24.0	0.4	3.0	2.8
MKD153-556.5	UQAC 2010	10.8	3.3	31.8	9.3	6.7	13.9	0.4	4.2	4.7
MKD153-556-568	Analabs 1995	14.0	6.0	34.0		9.0	13.0	0.4	2.2	3.8
MKD153-591.5	UQAC 2010	23.4	6.8	53.1	16.4	12.0	25.7	0.5	3.8	4.4
MKD153-589-592	Analabs 1995	13.0	5.0	35.0		9.0	18.0	0.5	3.6	3.9
MKD153-669.5	UQAC 2010	30.1	8.0	64.1	24.0	19.8	32.8	0.5	4.1	3.2
MKD153-669-671	Analabs 1995	29.0	8.0	53.0		14.0	22.0	0.4	2.8	3.8
MKD153-578.2	UQAC 2010	39.7	10.9	79.4	25.5	20.4	46.3	0.6	4.3	3.9
MKD153-576-579	Analabs 1995	25.0	7.0	53.0		11.0	25.0	0.5	3.6	4.8
Relative differences between determinations (square root of squared difference divided by average for each pair)										
MKD153-513-515 (%)		28.5	21.9	23.6		14.1	15.2	8.5	36.8	37.4
MKD153-643-645 (%)		13.7	11.6	4.0		41.5	14.7	10.7	26.2	45.4
MKD153-556-568 (%)		26.1	58.8	6.8		28.9	6.5	13.4	64.8	22.1
MKD153-589-592 (%)		57.3	29.9	41.0		28.7	35.2	6.1	5.4	12.7
MKD153-669-671 (%)		3.6	0.3	19.0		34.3	39.5	20.9	39.3	15.6
MKD153-576-579 (%)		45.4	43.4	39.9		59.9	59.7	21.0	17.4	21.2
Median (%)		27.3	25.9	21.3		31.6	25.2	12.0	31.5	21.7

Isotopes used: ^{101}Ru, ^{103}Rh, ^{106}Pd, ^{189}Os, ^{193}Ir, ^{195}Pt (note that samples are not exact replicates—UQAC samples are 40-cm quarter core grab samples from within original 2-m half-core composites analysed by Analabs)

Grguric et al. (2006). The ultramafic rocks of the Mount Keith Ultramafic Complex are pervasively altered to serpentine, with less abundant talc carbonate assemblages, and no igneous olivine is preserved. The rocks of the MKD153 profile are predominantly lizardite–brucite–hydrotalcite serpentinites with minor chlorite and carbonate, and accessory relic igneous chromite with secondary magnetite overgrowths or showing partial replacement by stichtite and woodallite (Grguric 2003). Serpentine–brucite assemblages form typical mesh textures with faithful pseudomorphing of original olivine grains. Carbonate, specifically ferroan magnesite, is characteristically present as intergrowths with chlorite in original interstitial liquid patches, and as rims and marginal intergrowths with sulphides (Fig. 3). Aside from thin rims on chromite and sulphide blebs, magnetite also forms fine dustings associated with mesh veins within olivine pseudomorphs.

Talc carbonate alteration is restricted to narrow and very sharply defined veins, up to 50 cm wide within serpentinite, and constitutes <5% of the interval. Mineralogy consists of talc, ferroan magnesite, and chlorite.

Interstitial sulphide blebs in serpentinites range in size from 40 μm to 1.5 mm and form interconnected branching tubes or channels at the triple point junctions of former olivine grains (Barnes et al. 2008). These blebs consist of aggregates of Ni–Fe sulphide grains in some cases surrounded by a corona of magnetite, the outer margins of which are partially replaced by iowaite, chlorian pyroaurite (± tochilinite), or ferroan magnesite in most cases. Blebs also commonly host irregular crosscutting veinlets of magnetite, common elsewhere in the deposit but relatively minor within this intersection. The sulphide mineralogy through the entire profile consists almost entirely of pentlandite, pyrrhotite, and minor chalcopyrite, with trace pyrite and minor magnetite developed as rims and fracture fills. Pentlandite forms coarse, blocky grains (Fig. 3), which in places appear to be fragmented and infilled with pyrrhotite (Fig. 3c). This texture is possibly attributable to volume expansion of the host rock during the serpentinization reaction (Barnes et al. 2009).

Geochemical profile

The MKD153 profile (Figs. 2 and 4) intersected a sequence of typical coarse-grained olivine adcumulates representing the whole of ore-bearing Unit 104 of Rosengren et al. (2007) and the top 15 m of underlying sulphide-poor Unit

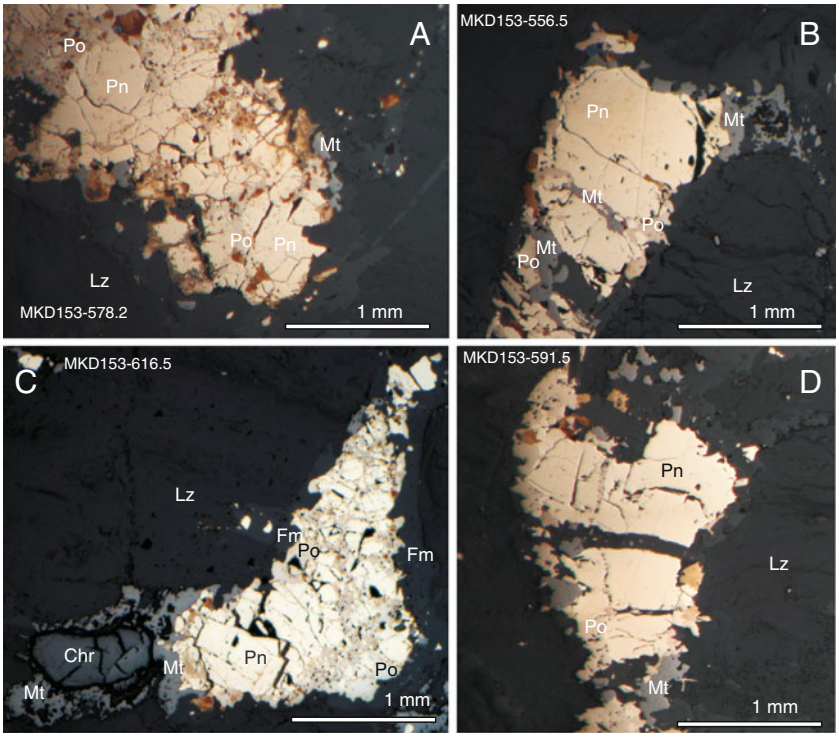

Fig. 3 Sulphide petrography. **a** Pentlandite (*pn*) and pyrrhotite (*po*) in lizardite with thin partial magnetite selvedge. **b** Same, with magnetite fracture fill or "cross-bar" and rim, intergrown with ferroan magnesite in top right. **c** Same, adjacent to chromite grain (*chr*) with extensive magnetite overgrowth. Pyrrhotite fills ramifying fracture network within pentlandite. **d** Pentlandite (*pn*) and pyrrhotite (*po*) in lizardite, magnetite as discrete grains at margin of sulphide, broad overgrowth of ferroan magnesite with magnetite inclusions

102. The upper 40 m of the intersection plotted in Fig. 4 includes the lowermost part of Unit 105, characterized by olivine mesocumulates, evident in the slightly higher Al contents. Within the entire intersection, trapped liquid contents in the cumulates are sufficiently low that whole rock compositions can be interpreted with confidence as

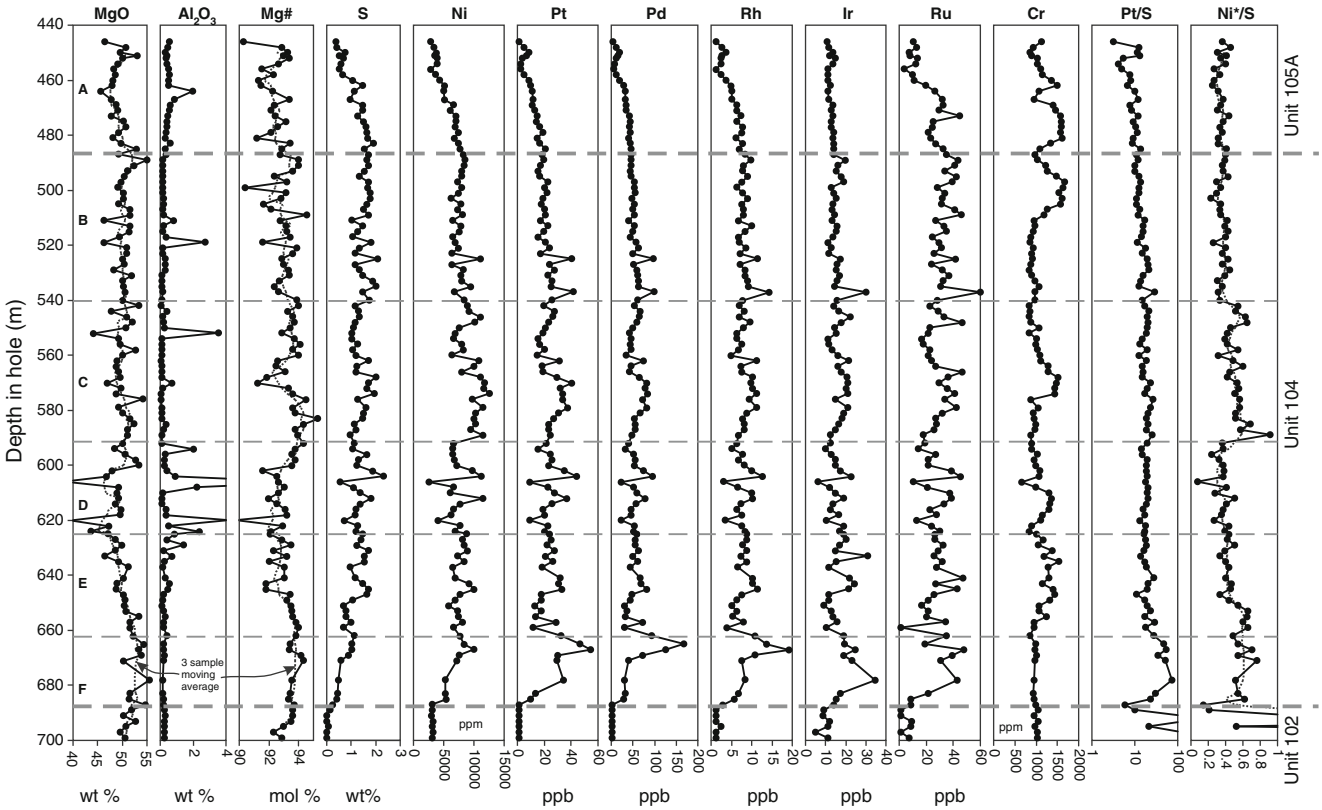

Fig. 4 Detailed geochemical profile down drill hole MKD153. Dashed trend lines are 3-sample moving average

simple two-component linear mixtures of olivine and magmatic sulphide liquid, locally with a small additional component of chromite. The exception is within thin intervals (usually <1 m) of coarse-grained orthocumulate, marked by elevated Al contents, referred to as "porphyritic olivine rock" (Dowling and Hill 1993) and thought to represent pockets or expulsion pathways of trapped intercumulus melt, probably analogous to the spinifex veins of Houle et al. (2009).

The intersection is divided into informal chemostratigraphic zones A to F (top to bottom) for the purposes of this study. The zone boundaries are somewhat arbitrary, but are defined primarily by combinations of fine-scale cyclicity in original olivine composition, defined by Mg#, and sulphide composition, defined by Pt/S and Ni*/S, where Ni* is whole rock Ni content less the estimated original average Ni content of the olivine component in each zone, as determined from the regression analysis described below (zone A—1,500 ppm, zone B—2,200 ppm, zones C and D—2,600 ppm, zone E—2,200 ppm, and zone F—2,800 ppm).

The base of zone F, the lowermost zone within mineralized Unit 104, is defined by the first appearance of cumulus sulphide and is marked by upward trends of increasing PGE, S, and Ni at a near constant olivine composition of $Fo_{93.6–93.9}$. The top of this interval and the base of zone E is the top of this increasing sulphide trend, which coincides with the onset of a steady drop in olivine composition (again, inferred from whole rock Mg#) of about 1 mol% Fo from $Fo_{93.9}$ towards $Fo_{92.8}$ at the top of zone E and base of zone D. This drop through zone E also corresponds to a slight but distinct trend of decreasing Ni*/S and Pt/S and an increase in Cu/Pd. Zone D retains the $Fo_{92.8}$ olivine composition, interrupted by a number of small porphyritic olivine rock units, and constant sulphide composition as inferred from Pt/S and Ni*/S.

The base of zone C corresponds to the top of an upward trend in Mg# and a distinct upward step in Ni*/S. Elevated and consistent Ni*/S persist through this 50-m interval of cyclically fluctuating Mg#. The top of zone C and base of zone B is barely discernible in Mg#, but is marked by a distinct downward step in Ni*/S and the onset of an interval of steadily declining Pt/S at constant Ni*/S that defines zone B. The top of zone B corresponds to the base of zone A and Unit 105. Zone A is marked by an interval of declining S and chalcophile metal contents and a consistent increase to higher Al contents marking a transition from extreme adcumulates to low-porosity mesocumulates. The drop in S and Ni to background levels defines the top of zone A.

Through the mineralized interval as whole, S distribution shows a remarkably symmetrical distribution, with a flat peak at around 1.2–1.5% S. A histogram of S abundances (Fig. 5) reveals a weakly skewed distribution with a mode at about 1.2% S, an average of 1.26%, median of 1.21%, and standard deviation of 0.5%. The median value, corresponding to 3.3 wt.% sulphide at 38% S, is higher by a factor of 3 than the value of around 1% sulphide expected for cotectic olivine–sulphide mass ratios during fractional crystallisation of a sulphide-saturated komatiite magma (Barnes 2007).

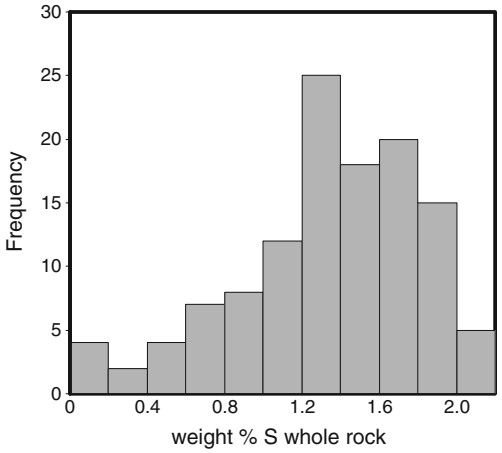

Fig. 5 Histogram of S abundance in the MKD153 profile

Inferred olivine compositions

Olivine compositions are inferred from a plot of whole rock Mg# (corrected for a component of Fe in sulphide (assuming an average of 18% Ni in sulphide and a monosulphide composition) vs. Al_2O_3. The plot (Fig. 6) shows calculated curves for olivine–liquid mixing lines assuming an initial komatiite magma composition of 30% MgO and 6% Al_2O_3, simple fractional crystallisation, and mixing of varying proportions of liquidus olivine with equilibrium trapped liquid based on the fractional crystallisation model of Barnes et al. (1995). These curves cannot be interpreted precisely, being based on calculations on the modelled differentiation products of a single parent magma, but they illustrate the very small magnitude of the change in olivine Mg# to be expected by equilibration between cumulus olivine and the very small amount of trapped liquid constrained by the very low Al contents of these cumulates. To a first approximation, the Mg# of the rock is the same as the original forsterite content of the olivine to within <0.2 mol% Fo for 95% of the samples. This conclusion carries the assumption that MgO contents of the rocks have not been greatly modified during alteration, a conclusion that is largely borne out by Pearce element ratio analysis of these rocks (Fiorentini et al. 2007), which indicates that they fall closely along pure olivine control trends in terms of molar ratios of Si to Mg + Fe.

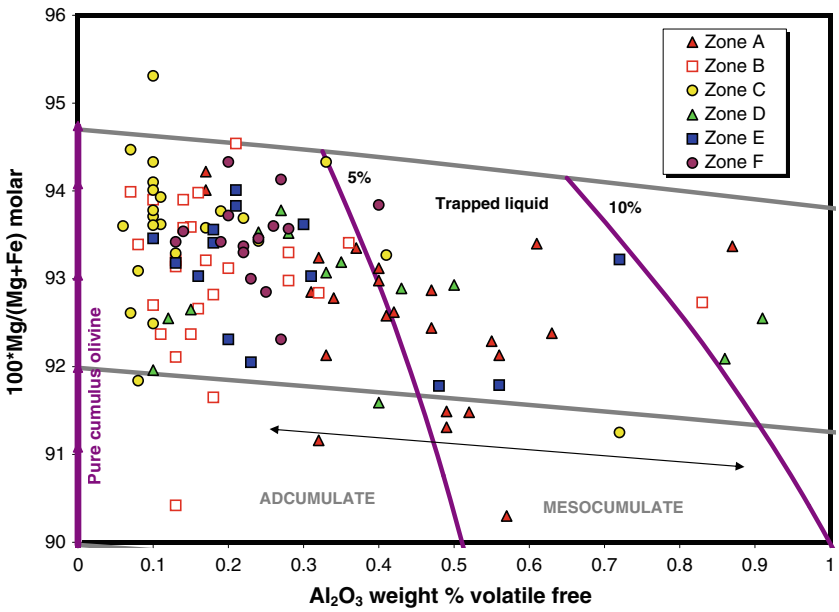

Fig. 6 Plot of Mg# vs. Al_2O_3 for MKD153 samples, by zone, compared with calculated curves for olivine–liquid mixing lines assuming an initial komatiite magma composition of 30% MgO and 6% Al_2O_3, simple fractional crystallisation, and mixing of varying proportions of liquidus olivine with equilibrium trapped liquid based on the fractional crystallisation model of Barnes et al. (1995)

Olivine compositions vary by as much as 2.5–3 mol% Fo within zones, but variation among different zones is subtle. Zones B to F contain the most forsteritic olivines, ranging up to $Fo_{94.6}$, corresponding to some of the most magnesian olivines known in komatiites and, hence, in most terrestrial rocks (Sobolev et al. 2007). Zones B to F are essentially identical to one another in olivine composition. Zone C contains the most extreme adcumulates, with <5% and as little as 2% trapped liquid, and zone D the least, although with <10% trapped liquid, these rocks would probably all be considered to be adcumulates by comparison to typical layered intrusion rocks. Zone A contains the distinctly less forsteritic olivines on average than the other units, but also ranges up to over Fo_{94}. In summary, the range of variation is small and relatively unsystematic. The range of olivines within each zone is larger than would be expected from simple fractional crystallisation, but there is no evidence of a simple monotonic upward decrease in forsterite content, as would be expected for a closed-system fractionation. The cumulate pile evidently crystallized in an open system, at least during the time interval recorded by zones F to B, in line with the usual interpretation of cumulate-rich komatiites.

Inter-element correlations between Ni, S, and PGEs

Correlations among whole rock Ni, S, PGEs, Co, and Cu are shown in Fig. 7 (which also allows a comparison between the main Analabs dataset and the small number of check analyses from Chicoutimi). Several of the individual zones show well-developed linear trends on Ni vs. S and PGE vs. S, whereas data for other zones tend to fall in between adjacent ones. Linear trends with positive nickel intercepts are particularly clear for Ni vs. S in zones A, D, C, and F; the Ni intercept at zero S decreases up section from about 3,000 ppm in zone F to about 1,600 ppm in A, and the slope of Ni vs. S also decreases systematically in the same order. The slope of Pt vs. S also decreases from F to A, but the Pt intercept at 0% S is indistinguishable from 0 ppb for all zones. Trends for Pd and Rh are similar, although less well defined for E, which is indistinguishable from B and C. In all these plots, zone B is somewhat chaotic and intermediate between the trends for zones C and A.

Trends are generally less well defined for Ru and Ir. Linear trends are still discernible for zones A, C, and F for Ru, with the Ru–S slope decreasing up sections from F to A, with near-zero intercepts. Zone C defines a weak linear trend with a slope indistinguishable from that of zone A. A similar pattern is evident on the Ir vs. S plots, with a well-defined zero-S intercept close to 10 ppb for both zones F and A. Zone A, in contrast, shows a very shallow, near-horizontal trend implying near independence of Ir on S.

The regression data in Table 4 can be used to estimate bulk compositions of the original sulphide liquid fraction of the rock, assuming an original S content of the sulphide liquid of 38% (calculated for a typical Ni-rich pyrrhotite/pentlandite ratio) and normalizing all elements shown in Fig. 7 up the appropriate regression line to this value (Table 5). Uncertainties are estimated using visual best fit minimum and maximum slopes to include approximately 90% of the data

Fig. 7 Correlations between whole rock Ni, S, PGEs, Co, and Cu ▶ subdivided by zone for the MKD153 sample profile. *Grey dashed line* on Ni vs. S is the ratio of Ni/S in stoichiometric pentlandite with Fe/Ni molar ratio of 1:1. Linear regression lines shown for zones A (*red*), C (*yellow*), D (*green*), and F (*purple*). *R* values and slopes are given in Table 4. Checked analyses from Univ. of Quebec (UQAC) indicated with crosses

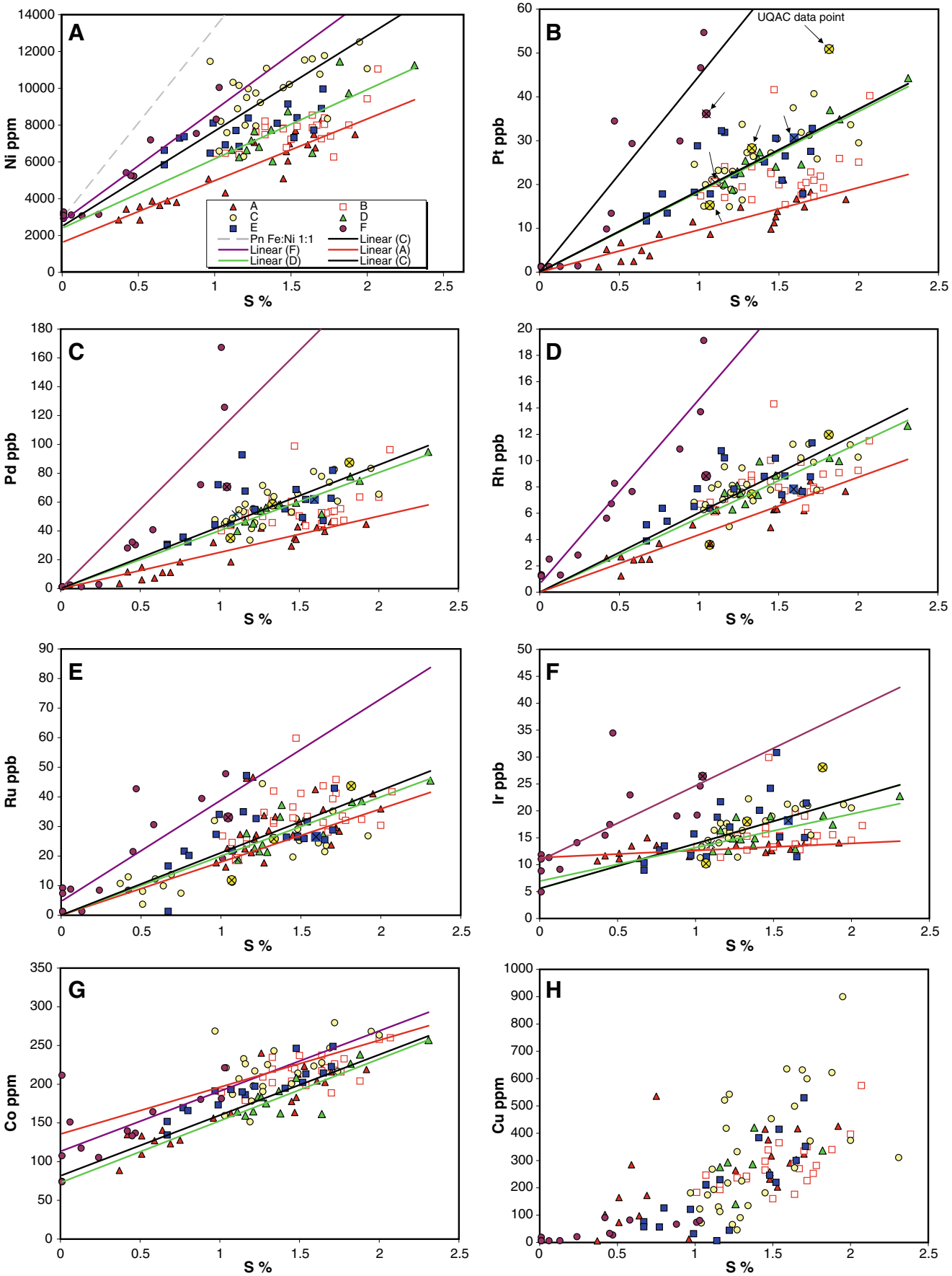
A
Ni ppm
S %
A
B
C
D
E
F
Pn Fe:Ni 1:1
Linear (F)
Linear (D)
Linear (C)
Linear (A)
Linear (C)
B
Pt ppb
UQAC data point
C
Pd ppb
D
Rh ppb
E
Ru ppb
F
Ir ppb
G
Co ppm
H
Cu ppm

Table 4 Regression statistics on inter-element plots shown in Fig. 7

Element	Zone	Intcpt	Slope	R^2	X S38	X 38 min	X 38 max
Ni	F	2,756	5,835	0.987	22.4	20.6	23.7
Ni	A	1,624	3,355	0.968	12.9	9.8	15.3
Ni	C	2,363	5,302	0.299	20.4	17.2	23.5
Ni	D	2,500	3,658	0.793	14.2	13.9	16.9
Pt	F	0	40.5	0.942	1539	1,121	1,824
Pt	A	0	9.76	0.954	371	293	418
Pt	D	0	18	0.71	684	612	752
Pt	C	0	18.82	0.874	715	600	825
Pd	F	0	96.6	0.892	3671	2,725	4,112
Pd	C	0	43	0.945	1634	1,406	1,820
Pd	D	0	40.4	0.96	1535	1,406	1,585
Pd	A	0	25.47	0.753	968	771	1,087
Rh	F	1	12	0.979	457	392	522
Rh	A	0	4.43	0.958	168	142	179
Rh	C	0	6.14	0.802	233	210	253
Rh	D	0	5.77	0.804	219	193	236
Ru	F	4	33.1	0.743	1,262	791	1,775
Ru	A	0	18.8	0.733	714	467	798
Ru	C	0	21.5	0.757	817	612	984
Ru	D	0	20.06	0.524	762	612	866
Ir	F	11	11.81	0.529	460	460	737
Ir	A	10	2.38	0.271	100	67	132
Ir	C	3	10.3	0.332	394	334	459
Ir	D	6	7	0.572	272	200	371

XS38 = element concentration extrapolated along regression line to 38% S, taken as the S content of pure sulphide liquid. Max and min based on minimum and maximum slopes of lines enclosing 90% of data points

in each set (not shown on the figures for reasons of clarity). This calculation involves a significant assumption of lack of post-igneous modification of all elements, but particularly S; this assumption demands some rigorous examination and is discussed further below.

A further set of inter-element correlations, based on non-overlapping averages of three consecutive samples (i.e. 6 m of core), is shown in Fig. 8 and gives an indication of the variability of element ratios in the sulphide fraction. The ratio Pt/Ni is variable, being highest in zone F and lowest in zone A with non-systematically fluctuating intermediate values in C (similar to A), D, and E (higher and similar to F, respectively). Correlations between Pt, Pd, and Rh are very strong, and the ratios of these elements to one another are indistinguishable for all zones, except A which has slightly higher Pd/Pt and Rh/Pt. Inter-element ratios of Rh, Ir, and Ru are much more erratic, particularly for Ru–Ir, although generally consistent within zones F, C, and A.

Discussion

S mobility during alteration

The derivation of sulphide tenors, that is, the calculated composition of the original average sulphide liquid com-

Table 5 Calculated sulphide tenors for zones of the Mount Keith MKD153 profile

Zone	Ni	+/−	Pd	+/−	Pt	+/−	Rh	+/−	Ru	+/−	Ir	+/−
A	12.9	4.3	968	255.9	371	101	168	32	714	289	100	49
C	20.4	4.7	1,634	321.1	715	169	233	33	817	289	394	93
D	14.2	1.6	1,535	153.9	684	106	219	35	762	203	272	122
F	22.4	2.5	3,671	1166.6	1,539	561	457	97	1,262	728	460	139
Perseverance dunite dissem sulphide (Barnes et al. 1988)	14.5	2.7	2,651	701.0	1,591	516	73	66	325	288	46	62

Uncertainty is derived from data in table

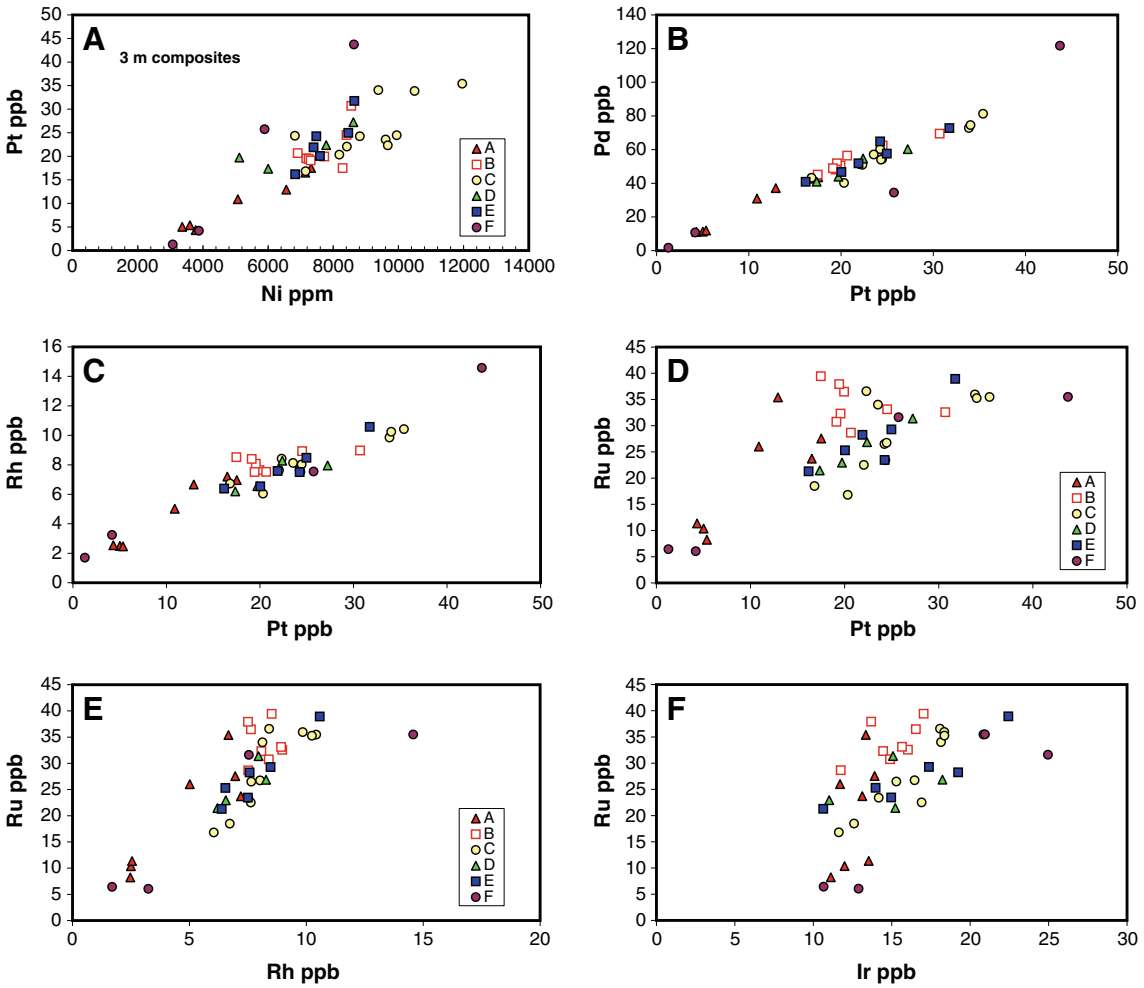

Fig. 8 Correlations between whole rock Ni and selected combinations of PGEs calculated as 3-sample averages over consecutive non-overlapping downhole intervals, subdivided by zone for the MKD153 sample profile

ponent of the various zones, is heavily dependent on the assumption that there has not been substantial redistribution of ore-forming elements during the serpentinization of the rocks. Crucially, it rests on the assumption of the immobility of S. This is counter to the current consensus on Mount Keith-type ores that their Ni tenor has been substantially upgraded as a result of oxidation of original pyrrhotite to magnetite (Grguric 2002; Grguric et al. 2006). Four lines of evidence point to this not being the case in the present sample set:

1. The evidence for pyrrhotite oxidation at Mount Keith is primarily the presence of very pentlandite-rich assemblages cut by magnetite veins referred to by Grguric et al. (2006) as "cross-bars". This is particularly evident in the sub-economic lower zone 102 of the complex, not sampled in this study. Although some evidence for veining and rimming of pentlandite by magnetite does exist in our zone 104 samples (for example Fig. 3b), it is nonetheless a relatively minor feature. Most of the magnetite in the samples forms rims rather than veins, and the magnetite that does occur in veins can be interpreted as fracture fill introduced during the serpentinization-induced volume expansion of the rock mass rather than as replacement. Pyrrhotite is universally present through the entire intersection, and shows no evidence of being unstable with respect to oxidation to magnetite. The observed assemblages are entirely consistent with primary magmatic compositions within the typical range observed in komatiite-hosted ores.
2. The Perseverance (formerly Agnew) deposit 60 km southeast of Mount Keith contains a large disseminated sulphide halo around a basal sulphide-rich type I ore accumulation. Much of this disseminated sulphide zone is developed within completely fresh unserpentinized dunite (Barnes et al. 1988) and consists of pentlandite-rich pyrrhotite–pentlandite–chalcopyrite assemblages, with very minor pyrite, very similar to those observed here. Compositions of the sulphide fraction of these rocks were inferred from whole rock analyses by

Barnes et al. (1988) using electron probe determinations to correct for Ni in olivine and are included in Table 5. Calculated Ni tenors are within error of those determined for zones A and F, although somewhat lower than those for zones C and F. Ni tenors in fresh, unserpentinized sulphide-bearing Perseverance dunites were determined in an earlier study by a selective sulphide leach process (Binns and Groves 1976). Ni tenors in pure sulphide ranged from 18.6% to 45% Ni, the higher value being found in a pentlandite–pyrite–millerite assemblage. Subsequently, similarly high Ni tenor pentlandite–millerite–pyrite assemblages with Ni tenors in the vicinity of 30% have been observed in completely unserpentinized dunite from the Betheno deposit at Yakabindie, 15 km south of Mount Keith (Barnes et al. 2011). High Ni tenor values in excess of 40% are unlikely to be primary magmatic tenors and are more likely to be controlled by an Fe–Ni exchange between olivine and sulphide (Binns and Groves 1976; Brenan and Caciagli 2000; Brenan 2003), but Barnes et al. (2011) present data on olivine zoning to show that the high Ni tenor at Betheno is a primary value and cannot be explained by olivine–sulphide exchange. These occurrences demonstrate that alteration of the host ultramafic rock is not necessary to generate Ni sulphide tenors in excess of 30%.

3. Sulphide tenors calculated for the Mount Keith ores correspond closely to values observed in other komatiite-hosted deposits, particularly those at Kambalda (Cowden et al. 1986), as discussed in more detail below.
4. The inter-element correlations between Ni, PGE, and S are remarkably strong, particularly in zones A and F. It is difficult to see how these correlations could be retained if S was mobile or had been systematically lost by oxidation. It is conceivable that high fluid/rock ratios could result in the buffering of specific Ni-rich sulphide assemblages such that the Ni content of the rock controlled the S content rather than the other way around, but this would only be possible if the sulphide assemblage was buffered in the pentlandite-only field (as it may well be in the more S-poor underlying zone 102). However, the variance in Ni in the MKD153 samples is related to varying pyrrhotite/pentlandite ratios, and whilst fluid buffering could constrain the sulphide composition to fall on pyrrhotite–pentlandite tie lines, it is not capable of constraining the relative ratios of these two phases.

On these lines of evidence, it is highly likely that S was not significantly mobile during serpentinization in the portion of the orebody sampled by hole MKD153, at least on a scale represented by the 2-m sample composites. The slopes of the metal vs. S regression lines are therefore reliable indicators of the original composition of the cumulus sulphide liquid component in the rock. This is not necessarily the same value, in the case of Ni, as the present tenor of the bulk sulphide assemblage as it is possible that redistribution of Fe and Ni may take place between olivine (or its alteration products) and sulphide subsequent to olivine and sulphide accumulation. This redistribution may arise from the release of original silicate Ni to sulphide during hydration of olivine to serpentine (e.g. Groves et al. 1974; Eckstrand 1975; Donaldson 1981; Hill and Gole 1990) or during subsolidus Fe–Ni exchange between olivine and sulphide in response to the changing equilibrium constant for the Fe–Ni exchange between these phases (Binns and Groves 1976; Brenan and Caciagli 2000; Brenan 2003).

Cumulate sulphide tenors of Mount Keith ores compared with other deposits

Compositions of the cumulus sulphide component in zones A, C, D, and F are compared in Fig. 9 with bulk compositions of a number of other komatiite-hosted Ni ore deposits using the data compilations of Naldrett (2004) and Barnes (2006). The Mount Keith data points fall in the middle of the cluster for each of the element pairs plotted and correspond closely to the trend defined by Kambalda bulk ores as originally defined by Cowden et al. (1986). Cumulus sulphide liquid compositions at Mount Keith were evidently entirely typical of the range for komatiite-hosted deposits (Table 5).

Chalcophile element patterns (PGEs plus Ni) are shown for zones A, C, D, and F in Fig. 10, with error bars determined at 90% confidence limits based on uncertainty in the regression slope. Uncertainties are high for the IPGE, and especially Ir, owing to the large uncertainty in the zero-sulphur intercept. Allowing for this uncertainty, patterns are flat with low PPGE/IPGE for all four zones, similar to the Kambalda average.

Anomalous aspects of the PGE tenor data are the apparently very low Ir tenors in zone A, and also the somewhat variable ratios of the elements Ir, Ru, and Rh (IPGE) to one another in contrast to the very strong correlations between these elements that are commonly observed. The apparent variability is at least in part due to the uncertainty in the zero-S intercept on the Ir and Ru vs. S plots, which in turn is probably related to alloy saturation effects and a minor inferred component of IPGE-rich PGM as cryptic inclusions in olivine (Keays 1982; Barnes and Fiorentini 2008). However, this cannot explain the remarkably constant value of whole rock Ir in zone A and the almost complete independence of Ir on sulphide content in this zone. It appears that the effective partition

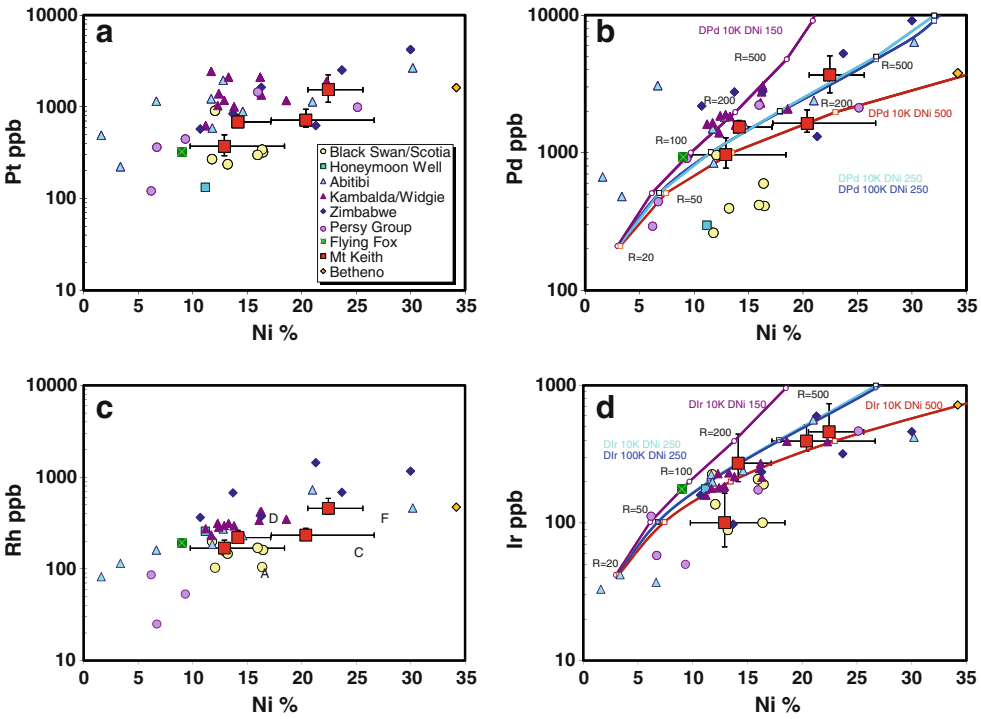

Fig. 9 Compositions of Mount Keith sulphides from zones A, C, D, and F expressed as element concentration in 100% sulphide compared with bulk deposit data from a variety of different deposits based on data compilations of Lesher and Keays (2002) and Barnes (2006) with additional data on Flying Fox from Collins et al. (2011) and from Betheno from Barnes et al. (2011). Model curves show compositions of magmatic sulphide component formed by bulk equilibration with komatiite magma with starting composition 1,600 ppm Ni, 10 ppb Pd, 1 ppb Ir, and 30% MgO at different values of *R* (indicated on frame *d*) and indicated constant values of sulphide/silicate partition coefficient for Ni, Pd, and Ir

coefficient for Ir into sulphide within this zone is much lower than that in other zones, or even that Ir is essentially non-chalcophile under conditions prevailing in zone A. This observation is currently unexplained, but it is possibly related to the dependence of partitioning on the position of the Ir–IrS sulfidation curve in fO_2–fS_2 space (Keays and Campbell 1981).

Evolution of the Mount Keith ore zone

The sulphide tenor results, coupled with the inferred olivine compositions derived above and other constraints from previous studies, constrain the magmatic evolution of the Mount Keith complex.

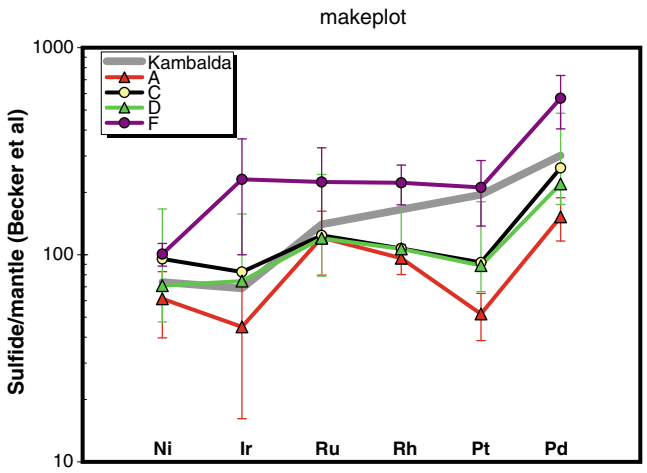

Fig. 10 Ni–PGE spidergrams for Mount Keith deposit zones compared with average bulk composition for Kambalda Dome shoots from Cowden et al. (1986)

A broad consensus exist that the S component of komatiite-hosted ores is primarily derived from crustal sources (see review by Lesher and Keays 2002), and this hypothesis is strongly supported at Mount Keith by S isotopic data. Non-mantle signatures are evident both in $^{34}S/^{32}S$ and in $^{33}S/^{32}S$, which shows evidence of mass-independent atmospheric fractionation (Bekker et al. 2009; Fiorentini et al. 2011). Externally derived S also accounts for the observation by Groves and Keays (1979) of very high S/Se ratios in Mount Keith ores; this observation was originally interpreted as a result of the addition of S during alteration, but is now regarded as a signature of crustally derived S (Lesher and Keays 2002). Lithophile trace element data also support extensive assimilation of felsic country rocks (Fiorentini et al. 2007).

The Mount Keith Ultramafic Complex evidently formed in an open system where successive (or continuous) pulses of magma fluctuated in composition during accretion or accumulation of the cumulus pile (Fig. 11). Fluctuation in olivine and sulphide composition reflect the processes of crystallisation in a dynamic conduit, with the slope of vertical profiles reflecting the balance between the rate of supply of new unfractionated magma and the change in magma composition with time along the flow axis. Based on microtextural features of olivine and sulphide droplets (Barnes 2007; Barnes et al. 2008), accumulation of the ore zone is thought to have involved a combination of in situ nucleation and growth of olivine at the floor of the flow coupled with

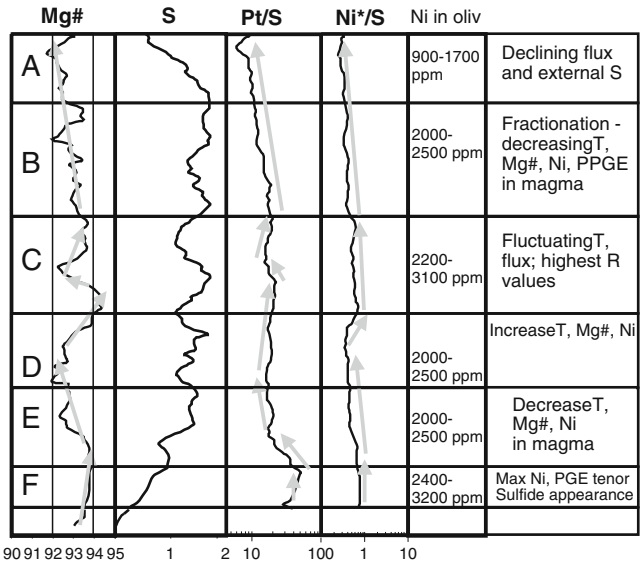

Fig. 11 Summary of olivine and sulphide composition variation through the Mount Keith ore zone in hole MKD153. Curves are 5-m rolling averages of each quantity; *arrows* are visual trend lines

mechanical sedimentation and deposition of transported sulphide droplets and an unknown proportion of olivine.

Zone F represents the gradual first appearance of a cumulus sulphide component of constant high Ni, IPGE, and PPGE derived from a previously sulphide-undersaturated magma with no previous history of PGE depletion, accounting for the mantle-like Cu/Pd ratio (Maier et al. 1998) within $Fo_{93.5}$ olivine adcumulates. Overlying zones E and D record a period of declining magma flux and temperature, marked by a trend to $Fo_{92.5}$ olivines with lower Ni and decreasing Ni and PGE tenors in sulphide. Zone C marks a period of increasing but variable magma flux and temperature, recorded by cyclically increasing forsterite contents up to $Fo_{94.5}$, and a step back to higher Ni tenors approaching those in zone F. Tenors of all PGE remain similar to those in D and E, suggesting a slight decrease in *R* value relating to a higher proportion of sulphide droplets entrained within the flowing magma. Ni and PPGE tenors become somewhat decoupled from one another, owing to significantly higher Ni but slightly lower Pt and Pd in the more primitive magma. This period is the peak period of magma flux through the Mount Keith conduit. The uppermost zones B and A represent a waning in magma flux and temperature, a gradual decrease in the rate of accumulation of cumulus sulphide liquid, and a progressive decrease in Ni and PGE tenors.

Modelling of magma, olivine, and sulphide liquid compositions

The geochemical trends summarized here can be investigated numerically using a variety of assumptions. Calculations have been carried out (Fig. 12) using three different sets of assumptions:

1. Simple addition and equilibration of an external FeS component, neglecting olivine crystallisation, and determining Ni and PGE contents of sulphide liquid using the conventional *R* factor equation of Campbell and Naldrett (1979) (simple *R* factor curves in Figs. 9 and 12), modified to account for external derivation of the sulphide component (Naldrett 1981; at the *R* values applicable here, this small refinement has a negligible effect on the calculations).
2. Assimilation–bulk equilibrium crystallisation (ABEC) model (Barnes et al. 1995) in which addition of FeS to form a sulphide liquid component is accompanied by equilibrium crystallisation of variable proportions of olivine. The calculation is performed using an iterative calculation constrained by an assumed variable partition coefficient for Ni between silicate

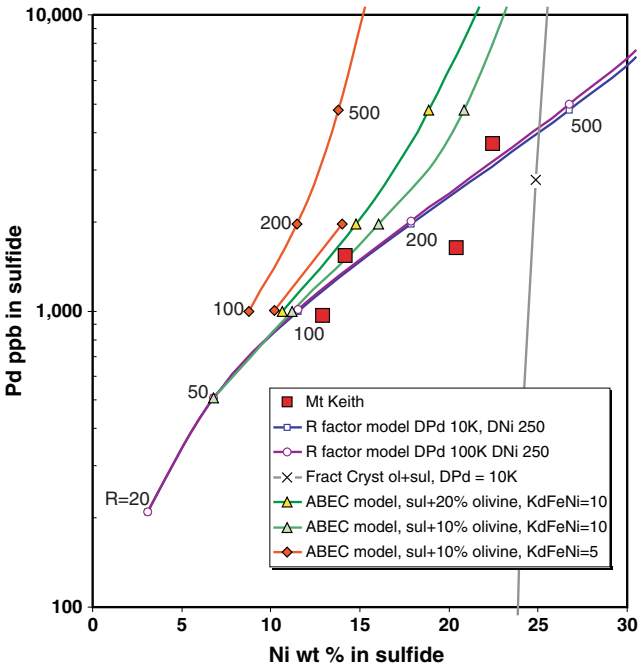

Fig. 12 Pd vs. Ni tenor data for Mount Keith zones A, C, D, and F compared with model trends. *R* factor trends same as that in Fig. 9. Assimilation and fractional crystallisation model trend from Barnes et al. (1995) for combined equilibrium sulphide segregation and olivine crystallisation at a mass ratio of olivine to sulphide of 40, similar to that observed in Mount Keith ores. FX trend is for pure fractional crystallisation of olivine and sulphide liquid in Mount Keith proportions for the same starting conditions of 1,600 ppm Ni and 10 ppb Pd in a 30% MgO komatiite starting composition. Ticks on FX curves are increments of 5% crystallisation. ABEC (assimilation and bulk equilibrium crystallisation) curves are calculated using the model method and assumptions of Barnes et al. (1995) and represent bulk equilibration of silicate magma and sulphide liquid in mass proportion *R* along with olivine at the indicated percentage of olivine to silicate melt. See text for further explanation

liquid and olivine and fixed distribution coefficients for Fe and Mg between silicate liquid and olivine, and for Fe and Ni between olivine and sulphide liquid. Details are given in the Appendix.

3. Fractional crystallisation of olivine and sulphide liquid, with liquidus phases removed as they form. This process is modelled as a series of incremental ABEC steps, with the final silicate liquid of each step fed in as input of the subsequent step.

The match of the sulphide tenor trend from zones F through to A to simple *R* factor or ABEC curves rather than to fractional crystallisation trends (Fig. 12) implies that this trend is predominantly controlled either by *R* factor variation (variable proportion of sulphide liquid) within a magma of constant composition or by a process of continuous bulk olivine crystallisation and sulphide liquid segregation. In the latter mechanism, which is essentially a perfect equilibrium crystallisation model, olivine and sulphide liquid are assumed to be continuously entrained and equilibrated in the magma as they form. The slope of the trend produced in Ni–Pd tenor space is broadly similar to, although somewhat steeper than that of, a pure R factor variation model and is very much less steep than trends produced for pure fractional olivine crystallisation and sulphide segregation, which predict extremely rapid rates of decrease of PPGEs relative to Ni and Cu for the proportions of olivine to sulphide observed within the Mount Keith ore zone. Varying the proportion of olivine to sulphide in the ABEC model by a factor of 2 makes a negligible difference to the sulphide liquid trajectory on the plots.

Distinguishing the pure *R* factor mechanism from the more complex equilibrium crystallisation mechanism on the basis of the model curves in Fig. 12 is not rigorous given the large number of degrees of freedom in the modelling. In particular, the Ni content of the sulphide liquid is strongly dependent on the sulphide/silicate partition coefficient for Ni, which in the model is determined by the assumed value of Fe/Ni K_d between olivine and sulphide liquid. The higher Ni ABEC curve corresponds to an assumed constant K_d of 10 and converges on the simple *R* factor curves which assume a constant sulphide/silicate partition coefficient of 250. The assumption of constant K_d is an oversimplification. Brenan (2003) and Brenan and Caciagli (2000) demonstrate that K_d is a complex function of fO_2 and the Ni content of the sulphide itself, giving rise to a complex nonlinear relationship beyond the scope of the simple ABEC model. However, the range of values chosen is within the range of those inferred from most natural komatiitic systems and is consistent with equilibration close to the QFM buffer at magmatic temperatures (Barnes et al. 2011).

The equilibrium crystallisation and assimilation (ABEC) model predicts a relationship between Ni and Pd tenor and olivine composition, which can be tested using the proxies of Ni/S and Pd/S (where Ni is corrected for estimated Ni in olivine using the zero-S intercept on the Ni vs. S regression for the various zones) and whole rock Mg# for olivine (Fig. 13). There is a very weak correlation through zones A to E for both Ni and Pd tenors with olivine composition (R^2 values of 0.14 and 0.13, respectively); however, a large proportion of the tenor variance is independent of olivine composition. This is consistent with the model curves in Fig. 13 which are calculated for the crystallisation of variable proportions of olivine for a given *R* value (determined by the proportion of sulphide liquid, assumed constant along each of the curves at 0.2, 0.5, and 1.0 wt.% sulphide). The curves show that for both Ni and Pd, tenors are controlled predominantly by *R* factor and equilibrium crystallisation of olivine has very little impact. For example, along the 0.2% sulphide curve, the effect of 20% equilibrium crystallisation of olivine is to reduce the sulphide tenor by a relative 15%. This implies that *R* factor fluctuations, interpreted as due to magma dynamics and supply of the assimilated S component from upstream, are predominantly responsible for the variance in sulphide tenor.

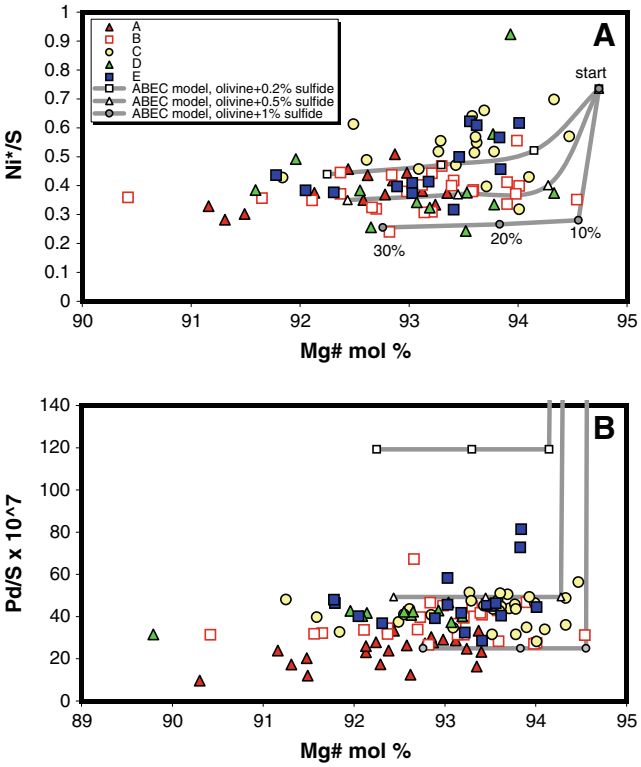

Fig. 13 Plots of whole rock Ni*/S (where Ni* is Ni corrected for estimated Ni in olivine using the zero-S intercept on the appropriate Ni vs. S regression for each zone) and Pd/S as proxies for Ni and Pd tenors of sulphide liquid, respectively, vs. whole rock Mg# as a proxy for olivine composition

PGE ratios in sulphide ores compared with komatiite magmas

Non-mantle ratios of PGEs in the Mount Keith ores (Fig. 10) require an explanation. It follows from the R factor equation of Campbell and Naldrett (1979)

$$Y_i^{\mathrm{f\,sul}} = X_i^{\mathrm{osil}} \cdot D_i^{\mathrm{sul/sil}} \cdot (R+1)/\left(R + D_i^{\mathrm{sul/sil}}\right) \quad (1)$$

that where values of R (silicate liquid/sulphide liquid mass ratio) is less than $10D_i^{\mathrm{sul/sil}}$, then the equation reduces to the approximation

$$Y_i^{\mathrm{sul}} \sim= X_i^{\mathrm{sil}} \cdot R \quad (2)$$

and hence that at low R values, the ratios of the high-D elements in the sulphide melt should be equal to the ratios in the silicate melt prior to sulphide equilibration. This point has been made in discussions of the origin of the Merensky Reef and other PGE-rich magmatic sulphide deposits (Cawthorn 1999; Cawthorn et al. 2005; Fonseca et al. 2009). It is widely accepted that $D_{\mathrm{PGE}}^{\mathrm{sul/sil}}$ values are at least of the order of tens of thousands (see review by Barnes and Lightfoot 2005) and R values as indicated by model trends in Fig. 9 are at least an order of magnitude lower. Hence, one would expect that the inter-element ratios of the PGEs to one another would be the same as those of the original komatiite magma prior to sulphide saturation. This hypothesis is tested in Fig. 14.

Fiorentini et al. (2011) have shown that the PGE patterns and abundances of komatiites of the same age and type (e.g., 2.7-Ga-old Al-undepleted komatiites) are remarkably similar worldwide and that unmineralized komatiites from the

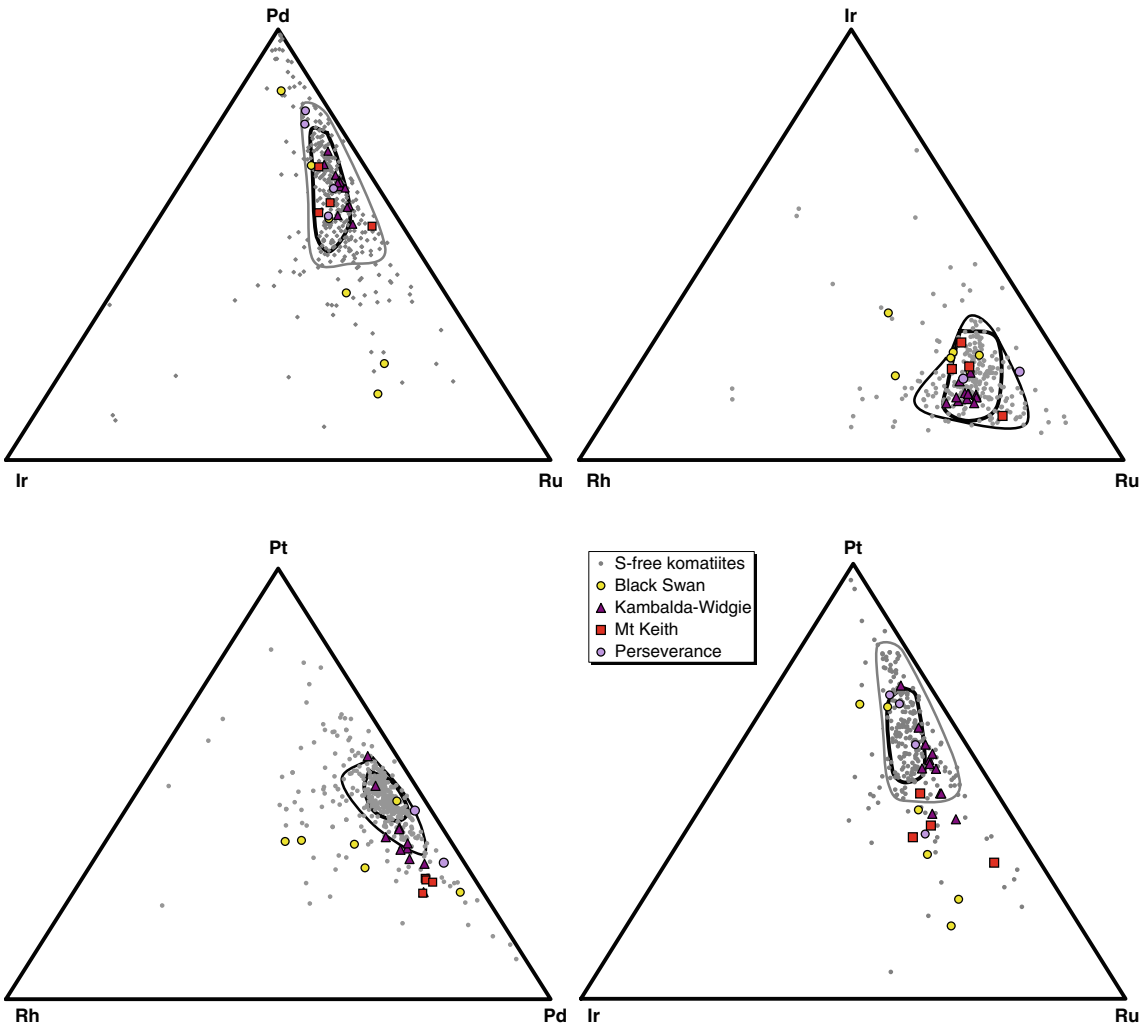

Fig. 14 Triangular plots (weight proportions) comparing relative proportions of different PGEs in bulk ore compositions from Mount Keith zones A, C, D, and F with those in typical Yilgarn Munro-type komatiites and other bulk sulphide ore compositions from the Kalgoorlie Terrane. Komatiite compositions: Al-undepleted (Munro-type) only, 15 < MgO < 35 (350 samples), contours show 50th and 80th percentiles on data density. Data sources: komatiite compositions from the compilation of Fiorentini et al. 2010; Kambalda-Widgiemooltha (Cowden et al. 1986); Black Swan (Barnes 2004); and Perseverance (Barnes et al. 1988)

Agnew-Wiluna domain fall squarely within the restricted global range. The dataset of unmineralized komatiitic rocks with MgO contents between 15% and 35% MgO is plotted in a series of triangular element proportion plots for various combinations of PGEs and contoured for data density using a triangular neighbour count algorithm. Bulk sulphide liquid composition estimates from various Kalgoorlie Terrane komatiite-hosted deposits, including Mount Keith, are superimposed.

With the exception of some massive sulphide ores from the Black Swan locality (an area of intense talc carbonate alteration), the proportions of Ir, Ru, Rh, and Pd in sulphide from all the deposits plotted, and the Mount Keith ores, match closely the silicate komatiite data. However, Pt is distinctly depleted relative to Pd, Rh, Ru, and Ir, and the trends on the Pt–Ru–Ir and Pt–Pd–Rh plots indicate that the mismatch is largely due to Pt depletion, not enrichment in the other PGE. The mismatch in Pt/Pd ratio is also evident from Figs. 8b and 15: Pt and Pd are very strongly correlated with one another and characteristically have a Pd/Pt ratio of close to 2 at Mount Keith and most of the other samples of disseminated ores shown in Fig. 15, whereas komatiites consistently have Pd/Pt very close to 1 (Puchtel and Humayun 2000, 2001, 2004; Fiorentini et al. 2011). A deficiency of Pt relative to Pd and the other PGEs appears to be a general characteristic of sulphide ores formed from komatiites of both sulphide-rich type I and sulphide-poor type II varieties.

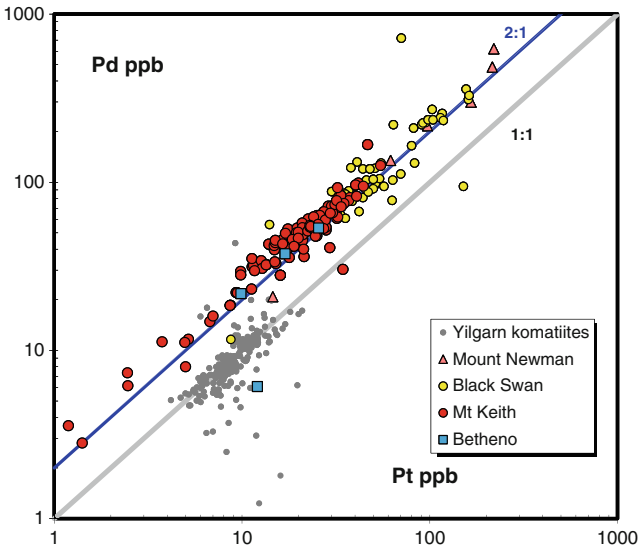

Fig. 15 Pt vs. Pd disseminated ores from the Kalgoorlie Terrane. Black Swan data include only the Black Swan and Cygnet disseminated orebodies (Barnes 2004). Mount Newman (unpublished CSIRO data) is a type IIB (blebby disseminated) deposit from the Mount Clifford area. Betheno dataset includes partially serpentinised and completely fresh dunite (Barnes et al. 2011). Komatiite data includes all unmineralized 2.7–2.9 Ga Al-undepleted samples with MgO between 15 and 35 wt.% anhydrous from compilation of Fiorentini et al. (2010)

A number of possible interpretations can be and have been offered for this Pt discrepancy, which has been noted primarily in massive ores in previous studies (Barnes 1998). The major candidates are: (1) radically different partition coefficients between Pt and the other PGE; (2) MSS fractionation (or some other form of mass sorting of MSS) within the sulphide pool; (3) selective hydrothermal mobility of Pt; (4) magmatic fractionation of Pt from other PGEs due to involvement of high-T magmatic Pt-rich phases; (5) addition of PGEs from external sources during assimilation; or (6) distinctly different diffusion characteristics of Pt in silicate melts relative to other PGEs, giving rise to effectively much lower D values. We consider these explanations in turn.

Partition coefficients

Distinctly different partition coefficients for Pt and Pd have been proposed by Vogel and Keays (1997) on the basis of geochemical analyses of the Newer Volcanic Province basalts in Victoria: They inferred $D^{sul/sil}$ values of 35,000 for Pd and 3,500–13,800 for Pt based on the degrees of depletion of these elements attributed to sulphide extraction. Leaving aside the model-dependent assumptions inherent in these numbers, and the applicability of the extrapolation from basalts to komatiites, the values for both Pt and Pd are still substantially less than the R values of <500 inferred for the Mount Keith sulphides (and for almost all other komatiitic systems). Hence, the condition that $R<<D$ still applies, and the ratio of the elements in sulphide liquid should still be closely similar to that in the original parent silicate magma.

From the argument arising from the D–R equation, Pt depletion could only be explained if the D value for Pt was at least two orders of magnitude lower than that for the other PGE. Pt depletion occurs in ores having R values of 100 or less, and a difference in D values would only become evident where D and R are of comparable magnitude, i.e. D_{Pt} would have to be <100. Values this low would then be inconsistent with strong covariance observed between Pt and the other PGEs in komatiitic deposits and the common occurrence of komatiitic sulphides containing parts per million levels of Pt.

MSS fractionation from sulphide liquid

The data presented here show that the negative Pt discrepancy is not restricted to massive ores and is clearly evident and highly consistent in disseminated ores also.

This observation suggests that an explanation involving MSS fractionation or accumulation (e.g. Barnes and Naldrett 1987), whilst it provides a good explanation for variable Rh/Pt in type I massive ores, cannot be the explanation for the more general phenomenon as there is no viable mechanism to produce MSS fractionation in dispersed disseminated sulphide droplets. Segregation of high-temperature Pt–As liquids or solid phases during sulphide solidification has been suggested as a mechanism to produce Pt enrichment (Hanley 2007), but as with MSS fractionation, it is difficult to envisage how this would be a viable mechanism in S-poor disseminated ores.

Hydrothermal mobility and dispersion

Hydrothermal mobility and dispersion of Pd and Pt have been called on in a number of previous studies (Lesher and Keays 1984, 2002; Seat et al. 2004; Stone et al. 2004), and it is certainly true that Pt and Pd tend to have a more erratic behaviour than the apparently highly immobile IPGE in altered magmatic sulphide ores (Barnes 2004). However, of the two elements, Pd generally appears to be the more soluble in hydrothermal fluids (Wood and Mountain 1991; Gammons and Bloom 1993; Gammons et al. 1993; Xiong and Wood 2000) and is more likely to be concentrated in hydrothermal Cu/Pd/Au-rich veins (Lesher and Keays 1984). The population of disseminated ores plotted in Fig. 15 includes samples from four different deposits with highly variable degrees and styles of alteration, including serpentinites, talc carbonates, and completely unserpentinized dunites from Betheno (Barnes et al. 2011). The remarkable consistency of the observed Pt/Pd ratio in these ores would require a highly selective mobility of precise proportions of Pt. Furthermore, these ores would have to lose Pt in the same proportion as the massive sulphide ores, which would presumably impose significantly different pH conditions on alteration fluids compared with those in sulphide-poor talc carbonates. The consistency of the Pd/Pt ratio can be taken as evidence of the relative immobility of both elements during the alteration of low-sulphide rocks, as noted at Black Swan in the remarkable preservation of strong Pt–MgO and Pd–MgO trends in sulphide-free, intensively talc carbonate altered komatiites (Barnes et al. 2004).

Magmatic fractionation of Pt from Pd

Fractionation of Pt from Pd, apparently unrelated to sulphide extraction, has been observed in some mafic magmatic suites including flood basalt suites from Greenland and Siberia (Lightfoot and Keays 2005; Momme et al. 2006), and this has led to the suggestion by these authors and others that sulphide liquid compositions may vary with the degree of fractionation as a result of compatible behaviour and prior depletion of Pt (Song et al. 2009). However, this explanation is difficult to reconcile with the known PGE geochemistry of komatiites, which evolve with a very consistent and constant Pt/Pd ratio very close to 1 (Puchtel et al. 2004; Fiorentini et al. 2010, 2011). It would also be expected that komatiites, being more primitive than basalts, should also show the minimum degree of fractionation-related Pt depletion. It fundamentally fails to explain the essential paradox that Pt/PGE ratios of komatiitic sulphides are systematically different from the very consistent values observed in the host magmas.

External derivation of PGEs

A review of the first draft of this manuscript suggested that PGE ratios may be modified by the addition of PGE from the external S source during the assimilation process which generated sulphide liquid. Brief consideration shows that this is untenable. The proportion of external sulphide added is limited by R factor considerations to <1%. In order to substantially modify PGEs in the silicate and sulphide melt, the PGE content of the assimilate would have to be at least 100 times greater than that of the komatiite magma, i.e. at parts per million levels. Furthermore, the PGE signal seen in the sulphides is one of Pt depletion, not Pd enrichment, so the external S source would have to be greatly enriched in Pd, Ru, and Rh. No data exist on the PGE contents of the likely Mount Keith S source, but it is highly unlikely that it contained parts per million levels of Rh and Ru.

Alternative mechanisms

In the absence of alternatives, an option that must be considered is that the partition coefficient, or at any rate its apparent effective value, may be systematically less for Pt than for the other PGEs under the conditions that apply in komatiite systems.

Kinetic processes, specifically diffusion of PGEs across compositional boundary layers around sulphide droplets, may play a role in limiting the effective partition coefficients of highly chalcophile species (Barnes 1993, 1998). This process has been considered quantitatively by Mungall (2002) who showed that complex variability in apparent partition coefficients could be modelled by variable diffusivities of different PGE species in the silicate melt, with Os, Ru, and possibly Pt being the most susceptible. On the evidence from komatiites, slow

diffusion of Pt in the melt may offer the best explanation of the consistent Pt deficiency in bulk sulphide ore compositions, and this mechanism may also account for some of the short-range variability in Ir/Ru, Rh/Ru, and Ir/Rh ratios evident between zones at Mount Keith. However, this explanation has some obvious defects in komatiitic systems. Komatiites are the highest temperature and lowest viscosity magmas known, and both these properties would be expected to give rise to high diffusion rates and to iron out any anomalous kinetic effects.

An alternative explanation is that under the conditions characteristic of sulphide-saturated komatiites, the *D* value for Pt is indeed orders of magnitude different from the other PGEs as a result of some discontinuous process. A candidate mechanism for this is a step change in the speciation of Pt in solution in the silicate melt. Brenan et al. (2003) suggested that the low tendency for Pt to partition into silicates such as olivine is due to speciation in the silicate melt as Pt^{4+}. Changes in speciation may be highly sensitive to fO_2 fluctuations related to interaction with sulfidic contaminants and could give rise to discontinuous changes in partitioning behaviour and a significantly different behaviour of PGEs from one another. This mechanism may also account for the non-chalcophile behaviour of Ir in subzone A. However, this aspect of PGE geochemistry remains poorly understood and awaits further experimental data on the precise nature of PGE speciation and behaviours in silicate magmas.

The problem of the Pt anomaly in komatiitic sulphides remains essentially unsolved. The issue is probably not restricted to komatiites; negative PGE discrepancies are widespread in other types of magmatic sulphide ores, for example those at Jinchuan (Song et al. 2009). Regardless of the precise mechanism, the data from the Mount Keith ores are strong evidence that the Pt discrepancy in komatiite ores, and possibly also in other settings, is a primary effect with a magmatic origin and not an artefact of alteration.

Conclusions

Based on strong correlations between Ni, PGEs, and S through the Mount Keith ore zone, the Ni and PGE tenors of type II Mount Keith sulphide ores have a range of values similar to the type I deposits of the Kambalda Dome. Mobility of S is evidently relatively minor at the scale of 2-m sample intervals.

Fluctuations in olivine composition indicate accumulation in a dynamic open system, interpreted as a high-flux magma conduit. Sulphide Ni and PPGE tenors vary together with, but somewhat decoupled from, inferred olivine composition through the ore zone. Tenor variations are predominantly controlled by *R* factor variations, with a minor component of variance from equilibrium crystallisation trends in the parent magma. PGE depletion due to sulphide liquid extraction is limited by entrainment of sulphide liquid droplets and continuous equilibration with the transporting silicate melt. Accumulation of the ore zone is thought to have involved a combination of in situ nucleation and growth of olivine at the floor of the flow, coupled with mechanical sedimentation and deposition of transported sulphide droplets.

Ratios of the PGEs to one another are similar to those in the host komatiite magma, consistent with an *R* factor control at values of *R* substantially less than the partition coefficients for the PGEs into sulphide liquid. The exception to this is Pt, which is systematically depleted in ores, relative to Rh and Pd and relative to host magma, by a consistent factor of about 2 to 2.5. This depletion matches that observed in bulk compositions of many komatiite-hosted orebodies. The highly consistent nature of this depletion, and particularly the very strong correlation between Pt, Pd, and Rh in the Mount Keith deposit, argues that this essentially unexplained depletion is a primary magmatic signal and not an artefact of alteration.

Acknowledgements The date on which this study was based originally formed part of an Honours thesis by Michael Fardon at Monash University supervised by Dr. Ray Cas and Dr. David Lambert and completed in 1995. We thank Jeff Foster and Nigel Brand, formerly with WMC Resources, and Terry Sweet, formerly with Analabs, for assistance in tracking down information on analytical procedures and quality control. The cooperation of BHP-Billiton has been essential for ongoing studies at Mount Keith and is gratefully acknowledged. Detailed studies of Mount Keith stratigraphy were carried out as part of AMIRA projects P710 and P710a. The paper has benefited from detailed discussions with Drs Ben Grguric and Belinda Godel. We thank Prof. Sarah-Jane Barnes and Dr D. Savard for the replicate PGE analyses from UQAC, which form part of an ongoing collaborative study between UQAC and CSIRO funded by the CSIRO Office of the Chief Executive. We acknowledge financial support (to MLF) from the Australian Research Council through grant LP0776780. Mike Lesher, Reid Keays, and an anonymous referee provided very helpful reviews. The paper is a product of the CSIRO Minerals Down Under National Research Flagship.

Appendix: geochemical modelling methods

The numerical models shown in Fig. 12 are simplified versions of the assimilation–bulk equilibrium crystallisation model described by Barnes et al. (1995), which solve equations for equilibrium distribution of Fe and Mg between silicate melt and olivine and for Fe and Ni between olivine and sulphide liquid for mass conservation, allowing for the addition of an externally derived FeS component whose proportion is defined by the input parameter *R*. The calculation was carried out iteratively in an Excel spreadsheet. The starting assumptions are as

follows: MgO, 30 wt.%; FeO, 9 wt.%; Ni, 1,600 ppm; Pd, 10 ppb; Ir, 2 ppb. $K_d^{(Fe/Mg)}$ for olivine/melt=0.30, $K_d^{(Fe/Ni)}$ for silicate/sulphide variable between 5 and 20. Fractional crystallisation is simulated as a series of incremental steps of 1% equilibrium crystallisation–segregation, with the finishing liquid composition of each step used as the starting composition for the next.

References

Barnes SJ (1993) Partitioning of the platinum group elements and gold between silicate and sulfide magmas in the Munni Munni Complex, Western Australia. Geochim Cosmochim Acta 57:1277–1290

Barnes SJ (1998) Possible causes of high Pd/Pt, Pd/Ir, Rh/Ir, Pd/Os ratios in sulfide ores. GAC-MAC Programs with Abstracts 1998, A9

Barnes SJ (2004) Komatiites and nickel sulfide ores of the Black Swan area, Yilgarn Craton, Western Australia. 4. Platinum Group element distribution in the ores, and genetic implications. Miner Depos 39:752–765

Barnes SJ (2006) Komatiite-hosted nickel sulfide deposits: geology, geochemistry, and genesis. Soc Econ Geol Spec Pub 13:51–118

Barnes SJ (2007) Cotectic precipitation of olivine and sulfide liquid from komatiite magma, and the origin of komatiite-hosted disseminated nickel sulfide mineralization at Mt Keith and Yakabindie, Western Australia. Econ Geol 102:299–304

Barnes SJ, Fiorentini ML (2008) Iridium, ruthenium and rhodium in komatiites: evidence for iridium alloy saturation. Chem Geol 257:44–58

Barnes S-J, Giovenazzo D (1990) Platinum-group elements in the Bravo intrusion, Cape Smith Fold Belt, northern Quebec. Can Miner 28:431–449

Barnes S-J, Lightfoot PC (2005) Formation of magmatic nickel sulfide deposits and processes affecting their copper and platinum group element contents. Economic Geologists 100th Anniversary Volume, pp 179–214

Barnes S-J, Naldrett AJ (1987) Fractionation of the platinum-group elements and gold in some komatiites of the Abitibi Greenstone Belt, Northern Ontario. Econ Geol 82:165–183

Barnes SJ, Gole MJ, Hill RET (1988) The Agnew Nickel Deposit, Western Australia: part II. Sulfide geochemistry, with emphasis on the platinum-group elements. Econ Geol 83:537–550

Barnes SJ, Lesher CM, Keays RR (1995) Geochemistry of mineralized and barren komatiites from the Perseverance Nickel Deposit, Western Australia. Lithos 34:209–234

Barnes SJ, Hill RET, Evans NJ (2004) Komatiites and nickel sulfide ores of the Black Swan area, Yilgarn Craton, Western Australia. 3. Komatiite geochemistry, and implications for ore forming processes. Miner Depos 39:729–751

Barnes SJ, Lesher CM, Sproule RA (2007) Geochemistry of komatiites in the Eastern Goldfields Superterrane, Western Australia and the Abitibi Greenstone Belt, Canada, and implications for the distribution of associated Ni–Cu–PGE deposits. App Earth Sci Trans Inst Min Metall B 116:167–187

Barnes SJ, Fiorentini ML, Austin P, Gessner K, Hough R, Squelch A (2008) Three-dimensional morphology of magmatic sulfides sheds light on ore formation and sulfide melt migration. Geology 36:655–658

Barnes SJ, Wells MA, Verrall MR (2009) Effects of magmatic processes, serpentinization and talc carbonate alteration on sulfide mineralogy and ore textures in the Black Swan disseminated nickel sulfide deposit, Yilgarn Craton. Econ Geol 104:539–562

Barnes SJ, Godel BM, Locmelis M, Fiorentini ML, Ryan CG (2011) Extremely Ni-rich Fe–Ni sulfide assemblages in komatiitic dunite at Betheno, Western Australia: results from synchrotron X-ray fluorescence mapping. Aust J Earth Sci (in press)

Bekker A, Barley ME, Fiorentini ML, Rouxel OJ, Rumble D, Beresford SW (2009) Atmospheric sulfur in Archean komatiite-hosted nickel deposits: Science 326:1086–1089

Beresford SW, Duuring P, Fiorentini ML, Rosengren N, Bleeker W, Barley, M, Cas R, Tait M, Wallace H (2004) The structural and stratigraphic architecture of the Agnew-Wiluna Belt, Western Australia. AMIRA P710A Final Report. AMIRA, Melbourne

Binns RA, Groves DI (1976) Iron–nickel partition in metamorphosed olivine–sulfide assemblages from Perseverance, Western Australia. Amer Miner 61:782–787

Brand NW (1997) Chemical and mineralogical characteristics of weathered komatiitic rocks, Yilgarn Craton, Western Australia: discrimination of nickel sulfide bearing and barren komatiites. Unpublished Ph.D. thesis, University of Western Australia, Nedlands, p 373

Brenan JM (2003) Effects of fO_2, fS_2, temperature, and melt composition on Fe–Ni exchange between olivine and sulfide liquid: implications for natural olivine–sulfide assemblages. Geochim Cosmochim Acta 67:2663–2681

Brenan JM, Caciagli NC (2000) Fe–Ni exchange between olivine and sulfide liquid: implications for oxygen barometry. Geochim Cosmochim Acta 64:307–320

Brenan JM, McDonough WF, Ash R (2003) Experimental constraints on the partitioning of rhenium and some platinum group-elements between olivine and silicate melt. Earth Planet Sci Lett 212:135–150

Brugmann GE, Naldrett AJ, Duke JM (1990) The platinum group element distribution in the Dumont Sill, Quebec; implication for the formation of Ni-sulfide mineralization. Mineral Petrol 42:97–119

Campbell IH, Naldrett AJ (1979) The influence of silicate:sulfide ratios on the geochemistry of magmatic sulfides. Econ Geol 74:503–1505

Cawthorn RG (1999) Platinum-group element mineralization in the Bushveld Complex—a critical reassessment of geochemical models. S Afr J Geol 102:268–281

Cawthorn RG, Barnes Stephen J, Ballhaus C, Malich KN (2005) Platinum group element, chromium and vanadium deposits in mafic and ultramafic rocks. Economic Geologists 100th Anniversary Volume, pp 215–249

Collins JE, Barnes SJ, Hagemann SG, McCuaig TC (2011) Variability in ore composition and mineralogy in the T4 and T5 ore shoots at the Flying Fox Ni–Cu–PGE Deposit, Yilgarn Craton, Western Australia. Econ Geol (in press)

Cowden A, Donaldson MJ, Naldrett AJ, Campbell IH (1986) Platinum group elements and gold in the komatiite-hosted Fe–Ni–Cu sulfide deposits at Kambalda, Western Australia. Econ Geol 81:1226–1235

Donaldson MJ (1981) Redistribution of ore elements during serpentinization and talc-carbonate alteration of some Archaean dunites, Western Australia. Econ Geol 76:1698–1713

Dowling SE, Hill RET (1992) The distribution of PGE in fractionated Archaean komatiites, Western and Central Ultramafic Units, Mt. Keith region, Western Australia. Austral J Earth Sci 39:349–364

Dowling SE, Hill RET (1993) The physical volcanology of komatiites of the Mt. Keith region, Norseman-Wiluna greenstone belt, Western Australia. In: Williams PR, Haldane JA (eds) International Conference on Crustal Evolution, Metallogeny and Exploration of the Eastern Goldfields, Australian Geological Survey Organisation, Canberra, pp 165–169

Eckstrand OR (1975) The Dumont serpentinite: a model for control of nickeliferous opaque assemblages by alteration products in ultramafic rocks. Econ Geol 70:183–201

Fardon M (1995) The effects of primary controls and post-depositional changes on the composition and mineralogy of komatiite-hosted nickel sulfide mineralization in the Norseman-Wiluna greenstone belt, Western Australia. Unpublished BSc thesis, Monash University, Melbourne, p 112

Fiorentini ML, Rosengren N, Beresford SW, Grguric B, Barley ME (2007) Controls on the emplacement and genesis of the MKD5 and Sarah's Find Ni–Cu–PGE deposits, Mount Keith, Agnew-Wiluna Greenstone Belt, Western Australia. Miner Depos 126:847–877

Fiorentini ML, Barnes SJ, Lesher CM, Heggie GJ, Keays RR, Burnham OM (2010) Platinum-group element geochemistry of mineralized and non-mineralized komatiites and basalts. Econ Geol 105:795–823

Fiorentini ML, Barnes Stephen J, Maier WD, Burnham OM, Heggie GJ (2011) Global variability in the platinum-group element contents of komatiites. J Petrol 52:83–112

Fonseca ROC, Campbell IH, O'Neill HSC, Allen CM (2009) Solubility of Pt in sulfide mattes: implications for the genesis of PGE-rich horizons in layered intrusions. Geochim Cosmochim Acta 73:5764–5777. doi:10.1016/j.gca.2009.06.038

Gammons CH, Bloom MS (1993) Experimental investigation of the hydrothermal geochemistry of platinum and palladium: III. The solubility of Ag–Pd alloy + AgCl in NaCl/HCl solutions at 300°C. Geochim Cosmochim Acta 57:2469–2479

Gammons CH, Yu Y, Bloom MS (1993) Experimental investigation of the hydrothermal geochemistry of platinum and palladium: II. The solubility of PtS and PdS in aqueous sulfide solutions to 300°C. Geochim Cosmochim Acta 57:2451–2467

Grguric BA (2002) Hypogene violarite of exsolution origin from Mount Keith, Western Australia: field evidence for a stable pentlandite–violarite tie line. Miner Mag 66:313–326

Grguric BA (2003) Minerals of the MKD5 nickel deposit, Mount Keith, Western Australia. Aust J Mineral 9:55–71

Grguric BA, Rosengren NM, Fletcher CM, Hronsky JMA (2006) Type II deposits: geology, mineralogy and processing of the Mount Keith and Yakabindie orebodies, Western Australia. Soc Econ Geol Spec Pub 13:119–138

Groves DI, Keays RR (1979) Mobilization of ore forming elements during alteration of dunites, Mt. Keith-Betheno, Western Australia. Can Miner 17:373–389

Groves DI, Hudson DR, Hack TBC (1974) Modification of iron–nickel sulphides during serpentinisation and talc-carbonate alteration at Black Swan, Western Australia. Econ Geol 69:1265–1281

Hanley JJ (2007) The role of arsenic-rich melts and mineral phases in the development of high-grade Pt–Pd mineralization within komatiite-associated magmatic Ni–Cu sulfide horizons at Dundonald Beach South, Abitibi Subprovince, Ontario, Canada. Econ Geol 102:305–317

Heath C, Lahaye Y, Stone WE, Lambert DD (2001) Origin of variations in nickel tenor along the strike of the Edwards lode nickel sulfide orebody, Kambalda, Western Australia. Can Miner 39:655–671

Hill RET, Gole MJ (1990) Nickel sulfide deposits of the Yilgarn Block. In: Hughes FE (ed) Geology of the mineral deposits of Australia and Papua New Guinea. Australasian Institute of Mining and Metallurgy, Melbourne, pp 557–559

Hill RET, Barnes SJ, Gole MJ, Dowling SE (1995) The volcanology of komatiites as deduced from field relationships in the Norseman-Wiluna greenstone belt, Western Australia. Lithos 34:159–188

Hill RET, Barnes SJ, Dowling SE (2001) Komatiites of the Norseman-Wiluna Greenstone Belt, Western Australia: a field guide. Western Australia Department of Mineral and Petroleum Resources, Perth, p 101

Houle MG, Prefontaine S, Fowler AD, Gibson HL (2009) Endogenous growth in channelized komatiite lava flows: evidence from spinifex-textured sills at Pyke Hill and Serpentine Mountain, Western Abitibi Greenstone Belt, Northeastern Ontario, Canada. Bull Volcanol 71:881–901

Hronsky JMA, Schodde RC (2006) Nickel exploration history of the Yilgarn Craton: from the Nickel Boom to today. Soc Econ Geol Spec Pub 13:1–11

Keays RR (1982) Palladium and iridium in komatiites and associated rocks: application to petrogenetic problems. In: Arndt NT, Nisbet EG (eds) Komatiites. George Allen and Unwin, London, pp 435–458

Keays RR, Campbell IH (1981) Precious metals in the Jimberlana Intrusion, Western Australia: implications for the genesis of platiniferous ores in layered intrusions. Econ Geol 76:1118–1141

Keays RR, Davidson RM (1976) Palladium, iridium and gold in the ores and host rocks of nickel sulfide deposits in Western Australia. Econ Geol 71:214–228

Keays RR, Ross JR, Woolrich P (1981) Precious metals in volcanic peridotite-associated nickel sulfide deposits in Western Australia, II. Distribution within ores and host rocks at Kambalda. Econ Geol 76:1645–1674

Keays RR, Nickel EH, Groves DI, McGoldrick PJ (1982) Iridium and palladium as discriminants of volcanic exhalative, hydrothermal and magmatic sulfide mineralization. Econ Geol 77:1535–1547

Lesher CM (1989) Komatiite-associated nickel sulfide deposits. In: Whitney JA, Naldrett AJ (eds) Ore deposition associated with magmas. Economic Geology Publishing, El Paso, pp 44–101

Lesher CM, Campbell IH (1993) Geochemical and fluid dynamic modelling of compositional variations in Archean komatiite-hosted nickel sulfide ores in Western Australia. Econ Geol 88:804–816

Lesher CM, Keays RR (1984) Metamorphically and hydrothermally mobilized Fe–Ni–Cu sulfides at Kambalda, Western Australia. In: Buchanan DL, Jones MJ (eds) Sulfide deposits in mafic and ultramafic rocks. Institute of Mining and Metallurgy, London, pp 62–69

Lesher CM, Keays RR (2002) Komatiite-associated Ni–Cu–PGE deposits: geology, mineralogy, geochemistry and genesis. In: Cabri LJ (ed) The geology, geochemistry mineralogy and mineral beneficiation of platinum group elements. Canadian Institute of Mining and Metallurgy and Petroleum Special Volume 54, pp 579–617

Lightfoot PC, Keays RR (2005) Siderophile and chalcophile metal variations in flood basalts from the Siberian Trap, Noril'sk Region: implications for the origin of the Ni–Cu–PGE Sulfide ores. Econ Geol 100:439–462

Maier WD, Barnes Stephen J, Dewaal SA (1998) Exploration for magmatic Ni–Cu–PGE sulfide deposits—a review of recent advances in the use of geochemical tools, and their application to some South African ores. S Afr J Geol 101:237–253

Momme P, Tegner C, Brooks CK, Keays RR (2006) Two melting regimes during Paleogene flood basalt generation in East Greenland: combined REE and PGE modelling. Contrib Mineral Petrol 151:88–100

Mungall JE (2002) Kinetic controls on the partitioning of trace elements between silicate and sulfide liquids. J Petrol 43:749–768

Naldrett AJ (2004) Magmatic sulfide deposits: geology, geochemistry and exploration. Springer, Heidelberg, p 727

Puchtel IS, Humayun M (2000) Platinum group elements in Kostomuksha komatiites and basalts: implications for oceanic crust recycling and core–mantle interaction. Geochim Cosmochim Acta 64:4227–4242

Puchtel IS, Humayun M (2001) Platinum group element fractionation in a komatiitic basalt lava lake. Geochim Cosmochim Acta 65:2979–2993

Puchtel IS, Humayun M, Campbell AJ, Sproule RA, Lesher CM (2004) Platinum group element geochemistry of komatiites from the Alexo and Pyke Hill areas, Ontario, Canada. Geochim Cosmochim Acta 68:1361–1383

Rödsjö L (1999) The alteration history of the Agnew-Wiluna Greenstone Belt, Western Australia, and the impacts on nickel sulfide mineralization. Ph.D. thesis, University of Western Australia, Nedlands, 185 pp

Rosengren NM, Beresford SW, Grguric BA, Cas RAF (2005) An intrusive origin for the komatiitic-dunite hosted Mount Keith disseminated nickel sulfide deposit, Western Australia. Econ Geol 100:149–156

Rosengren NM, Grguric BA, Beresford SW, Fiorentini ML, Cas RAF (2007) Internal stratigraphic architecture of the komatiitic dunite-hosted MKD5 disseminated nickel sulfide deposit, Mount Keith Domain, Agnew-Wiluna Greenstone Belt, Western Australia. Miner Depos 126:821–845

Ross JR, Keays RR (1979) Precious metals in volcanic-type nickel sulfide deposits in Western Australia. I. Relationship with the composition of the ores and their host rocks. Can Miner 17:417–435

Seat Z, Stone WE, Mapleson DB, Daddow BC (2004) Tenor variation within komatiite-associated nickel sulfide deposits: insights from the Wannaway Deposit, Widgiemooltha Dome, Western Australia. Mineral Petrol 82:317–339

Sobolev A, Hoffman A, Kuzmin D, Yaxley G, Arndt N, Chung S-L, Danyushevsky L, Elliott T, Frey F, Garcia M, Gurenko A, Kamenetsky V, Kerr A, Krivolutskaya N, Matvienkov V, Nikogosian I, Rocholl A, Sigurdson I, Sushchevskaya N, Teklay M (2007) The amount of recycled crust in sources of mantle-derived melts. Science 316:412–417

Song XY, Keays RR, Zhou MF, Qi L, IhIenfeld C, Xiao JF (2009) Siderophile and chalcophile elemental constraints on the origin of the Jinchuan Ni–Cu–(PGE) sulfide deposit, NW China. Geochim Cosmochim Acta 73:404–424

Stone WE, Heydari M, Seat Z (2004) Nickel tenor variations between Archaean komatiite-associated nickel sulfide deposits, Kambalda ore field, Western Australia: the metamorphic modification model revisited. Mineral Petrol 82:295–316

Vogel DC, Keays RR (1997) The petrogenesis and platinum-group element geochemistry of the Newer Volcanic Province, Victoria, Australia. Chem Geol 136:181–204

Wood SA, Mountain BW (1991) Hydrothermal solubility of palladium in chloride solutions from 300°C to 700°C: preliminary experimental results—a discussion. Econ Geol 86:1562–1563

Xiong Y, Wood SA (2000) Experimental quantification of hydrothermal solubility of platinum-group elements with special reference to porphyry copper environments. Mineral Petrol 68:1–28